Supplementary Materials

Biomimetic synthesis of sub-20 nanometer Covalent Organic Frameworks in water

Authors

Carlos Franco[1]†, David Rodríguez-San-Miguel[2]†, Alessandro Sorrenti[1], Semih Sevim[1], Ramon Pons[3], Ana E. Platero-Prats[2], Marko Pavlovic[4,5], Istvan Szilágyi[4,6], M. Luisa Ruiz Gonzalez[7], José M. González-Calbet[7], Davide Bochicchio[8], Luca Pesce[8], Giovanni M. Pavan[8,9], Inhar Imaz[10], Mary Cano-Sarabia[10], Daniel Maspoch[10,11], Salvador Pané[12], Andrew J. deMello[1], Felix. Zamora[2]*, Josep Puigmartí-Luis[1]*

Affiliations

[1]Department of Chemistry and Applied Biosciences, Institute for Chemical and Bioengineering, ETH Zurich, Vladimir Prelog Weg 1, 8093 Zurich, Switzerland.

[2]Departamento de Química Inorgánica, Institute for Advanced Research in Chemical Sciences (IAdChem) and Condensed Matter Physics Institute (IFIMAC). Universidad Autónoma de Madrid, 28049 Madrid, Spain.

[3]Institute for Advanced Chemistry of Catalonia (IQAC-CSIC), Jordi Girona 18-26, E-08034 Barcelona, Spain.

[4]MTA-SZTE Lendület Biocolloids Research Group, University of Szeged, H-6720 Szeged, Hungary.

[5]Max-Planck Institute of Colloids and Interfaces; Department of Colloid Chemistry, Am Mühlenberg 1, 14476 Potsdam, Germany

[6]Interdisciplinary Excellence Center, Department of Physical Chemistry and Materials Science, University of Szeged, H-6720 Szeged, Hungary.

[7]Departamento de Química Inorgánica, Universidad Complutense de Madrid, 28040 Madrid, Spain.

[8]Department of Innovative Technologies, University of Applied Sciences and Arts of Southern Switzerland, Galleria 2, Via Cantonale 2c, CH-6928 Manno, Switzerland.

[9]Department of Applied Science and Techology, Politecnico di Torino, Corso Duca degli Abruzzi 24, 10129 Torino, Italy.

[10]Catalan Institute of Nanoscience and Nanotechnology (ICN2), CSIC and BIST Campus UAB, Bellaterra, 08193 Barcelona, Spain.

[11]ICREA, Pg. Lluís Companys 23, 08010 Barcelona, Spain.

[12]Multi-Scale Robotics Lab ETH Zurich Tannenstrasse 3, CH-8092 Zurich, Switzerland.

*Correspondence to: felix.zamora@uam.es, jpuigmarti@ethz.ch

† These authors contributed equally to this work.

This PDF file includes:

Other Supplementary Materials for this manuscript include the following:

Materials and Methods

Materials

1,3,5-benzenetricarboxaldehyde was obtained from Manchester Organics, 1,3,5-tris(4'-aminophenyl)benzene (**TAPB**) was prepared according to published procedures.[1] 4,4',4"-(1,3,5-triazine-2,4,6-triyl)trianiline was obtained from Fluorochem. Other chemicals and solvents were obtained from Sigma Aldrich and used without further purification unless specified.

Attenuated Total Reflection Fourier Transform Infrared Spectroscopy

ATR-FT-IR spectroscopy was performed using a Perkin Elmer Spectrum 100 with a PIKE Technologies MIRacle Single Reflection Horizontal ATR accessory having a spectral range of 4000-650 cm^{-1}.

Solid-State ^{13}C CP-MAS Nuclear Magnetic Resonance Spectroscopy

Solid State NMR spectra were recorded at room temperature on a Bruker AV 400 WB spectrometer using a triple channel, 4 mm probe with zirconia rotors and a Kel-F cap. Cross-polarization with Magic Angle Spinning (CP-MAS) was used to acquire ^{13}C data at 100.61 MHz. The spectral width of the pulse sequence was 35 kHz and the ^{1}H excitation pulse was 3 μs. The CP contact time was 3.5 ms. High power two-pulse phase modulation (TPPM) ^{1}H decoupling was applied during data acquisition using a decoupling frequency of 80 kHz. Recycle delays were 4 s and the sample spinning rate was 10 kHz.

Thermogravimetry

Thermogravimetric analyses of samples were performed using a Thermobalance TGA Q-500 thermal gravimetric analyzer from TA Instruments, with samples held in a platinum pan under a nitrogen atmosphere. A 10 K min^{-1} ramp rate was used.

Elemental Analysis

Elemental analyses were obtained using LECO CHNS-932 elemental analyzer.

Field-Emission Scanning Electron Microscopy

Field-emission scanning electron microscopy (FE-SEM) images were collected on a Zeiss Ultra 55 scanning electron microscope at an acceleration voltage of 5.0 kV. Samples were coated with a mixture of Pt/Pd using a Quorum Q150T-S sputter coater.

Transmission Electron Microscopy

High-resolution transmission electron microscopy (HRTEM) images were obtained using a *JEOL-JEM GRAND ARM 300cF* microscope equipped with a Cs Corrector (ETA-JEOL). A precise measurement of aberrations and an optimized correction were achieved using JEOL COSMO corrector control software. The accelerating voltage was set to 60 kV in order to minimize sample damage. HRTEM images were acquired using a Gatan OneView CMOS camera (4096 x 4096 pixels).

Dynamic Light Scattering

DLS measurements were carried out using a Vasco 1 particle size analyzer from Cordouan Technologies.

Dynamic Light Scattering kinetics

To determine temporal changes in the hydrodynamic radii, DLS experiments were carried out using an ALV/CGS-8F goniometer equipped with a solid state Verdi2 laser operating at a wavelength of 532 nm. Measurements were carried out at 90^{o} scattering angle and the correlation function collected for 20 seconds. Cumulant analysis was used to determine the translational diffusion coefficient, which in turn was used to extract the hydrodynamic radius via the Stokes-Einstein equation.[2] For sample preparation, micellar solutions of 1,3,5-triformylbenzene (**BTCA**) and **TAPB** monomers were prepared first in either CTAB or CTAB/SDS (97:3) in water. DLS experiments were performed by merging 750 µL of micellar solution containing **BTCA**, 750 µL of **TAPB**-containing micellar solution and 75 µL of acetic acid (or MilliQ water for samples without catalyst). The final concentration of DLS sample was composed of 0.1 M CTAB surfactant (in addition to 0.0036 M SDS in the case of the mixed micelles), 0.8 M acetic acid and equal amount of two monomers at a concentration of 0.00125 M. The solution was immediately placed in a sample holder and the increase in micelle size was monitored in the presence or absence of acetic acid. The time-resolved measurements were performed during the first 3 hours after mixing.

Powder X-ray Diffraction

Standard PXRD patterns were collected with a Bruker D8 Advance X-ray diffractometer (Cu-Kα radiation; λ = 1.5418 Å) equipped with a Lynxeye detector. Samples were mounted on a flat glass sample plate. Patterns were collected with a step size of 0.032^{o} and an exposure time of 1.4 s/step.

Synchrotron X-ray diffraction data of COF suspensions

Synchrotron X-ray diffraction data were collected at the P02.1 beamline at PETRA IIII (Hamburg, Germany) using 60 keV (0.207 Å) X-rays. Samples were loaded into borosilicate capillaries as liquids and sealed using epoxy. Data were collected using an amorphous silicon-based PerkinElmer area detector. Geometric corrections and reduction to one-dimensional data were performed using DAWN Science software.[3–5] Differential diffraction analyses were performed by subtracting the signal of the solvent from that of the colloidal solution containing **TAPB-BTCA COF**, thereby enhancing the diffraction features of **TAPB-BTCA COF**. The colloid used for recording the XRD pattern was prepared following the general procedure described below, but using CTAB and SDS aqueous solutions of 0.001 M concentration.

Synchrotron X-ray diffraction data of MIL-100(Fe) suspensions

Synchrotron X-ray diffraction patterns of **MIL-100(Fe)** colloidal solutions were collected at the XALOC-BL13 beamline at Alba synchrotron. The colloidal solutions were first sealed in a glass capillary and centrifuged in the same capillary to have the higher density of nanoparticles at the bottom of the capillary. The experiment was carried out in transmission mode using a radiation with a wavelength, λ = 0.82653 Å directing the beam at the bottom of the capillary, with higher density of nanoparticles. Data were collected using a PILATUS 6M DECTRIS detector. The collected data were transformed using FIT2D program.

Gas Adsorption

Nitrogen adsorption and desorption measurements were done at 77 K using an Autosorb-IQ-AG analyser (Quantachrome). CO_2 Adsorption and desorption measurements were done at 203 K and 298 K using an ASAP 2020 HD (Micromeritics). Temperature was controlled by using a liquid

nitrogen bath. Gravimetric water vapor sorption isotherms were measured using a DVS vacuum instrument (Surface Measurement Systems Ltd). The weight of the dried powder (~ 20 mg) was constantly monitored with a high- resolution microbalance (± 0.1 μg) and recorded at 25 °C (± 0.2 °C) under pure water vapor pressures.

Small Angle X-ray Scattering

SAXS measurements were performed using a S3-MICRO (Hecus X-ray systems GMBH Graz, Austria) using a GENIX-Fox 3D X-ray source (Xenocs, Grenoble), delivering a detector focused X-ray beam (λ = 0.1542 nm, Cu Kα-line with more than 97% purity and less than 0.3% Kβ). X-rays were detected by means of a PSD 50 Hecus. The liquid sample was injected in a flow-through glass capillary (1 mm diameter and 10 μm wall thickness Hilgenberg Mark glass Nº4) kept in vacuum, with the temperature set to 30 ºC by a TCCS-3 Hecus Peltier system. The system was calibrated by measuring a standard silver behenate sample and put in absolute intensity by comparison with water.[6] Because of the use of a detector focused small beam (300 x 400 μm full-width at half-maximum), scattering curves are smeared by the detector width and depth. The instrumentally smeared experimental SAXS curves were fitted to numerically smeared models for beam size and detector width effects, with a least-squares routine based on the Levenberg-Marquardt algorithm being used.[7] The raw profiles were summed and binned for five consecutive channels to increase the signal-to-noise ratio. Due to that in the first two hours of measurements the SAXS signal intensity does not significantly change, we used these measurements to extract the background signal for the subsequently times.

Critical point drying

The solid wet with ethanol was transferred into a piece of dialysis tubing (Spectra/Por 1, MWCO: 6-8 kD) and then sealed. The membrane was then introduced into the critical point drying equipment. Critical point drying was performed in a SPI-DRY Critical Point Dryer - Jumbo by filling the chamber containing the sample with liquid CO_2 at 12 ºC, and allowing it to exchange for 1 hour, followed by flushing with fresh liquid CO_2. This solvent exchange procedure was performed a total of 5 times. After the final one, the temperature was raised up to 40 ºC to exceed the critical point of CO_2. Once this temperature was reached and CO_2 was in a supercritical state, the chamber was slowly vented at a rate of 10 bar h^{-1} until atmospheric pressure was reached and the sample could be recovered.

Cryo-TEM

COF particles were examined by cryogenic transmission electron microscopy (cryo-TEM) using a JEOL-JEM 2011 microscope (JEOL, Japan) operating at 200 kV. The samples were prepared in a controlled environment vitrification system. A 5-μl aliquot of each one was deposited onto carbon-coated film meshes supported by standard copper TEM grids. After 30 s, the grids were gently blotted with a double layer of filter paper to obtain a thin film (thickness: 20–400 nm), plunged into liquid ethane at its freezing point (−180°C), and then transferred into liquid nitrogen (−196°C), where they were stored until use. At that time, the vitrified specimens were transferred to the microscope using a cryo-transfer and its workstation (Gatan 626 DH, Gatan).

Coarse grain MD simulations

The coarse grained model for the **TAPB-BTCA COF** layer has been built in the framework of the well-known MARTINI force field.[8] We have used small MARTINI beads with a 2:1 mapping (2

heavy atoms into 1 CG bead) for the whole **TAPB-BTCA COF** layer. We have used SC5 beads to represent all the aromatic rings and all the beads containing nitrogen atoms, as previously done for another system,[9] and SP1 beads to represent all the beads containing an oxygen atom. The CG **TAPB-BTCA COF** layer has been mapped from its all atom structure using an in house python script.

The molecular dynamics simulations have been conducted with the Gromacs MD suite (2018 series).[10] We have placed 1 **TAPB-BTCA COF** layer in a simulation box and we added enough solvent (water or hexadecane) to completely solvate it. Then we constructed simulation boxes containing 3 or 10 stacked layers adding 3x or 10x the number of solvent molecules present in the 1 layer system. Simulations have been run in NPT conditions at 310 K and 1 atm of pressure using a time step of 10 fs and isotropic pressure scaling. All the other run parameters present in the mdp file have been set as in standard MARTINI simulations.

Supplementary Text

Synthesis of sub-20 nanometer **TAPB-BTCA COF** particles

23.3 mg of benzene-1,3,5-tricarboxaldehyde are dissolved in 0.25 mL of DMSO. This solution is added dropwise to 58 mL of an aqueous 0.1 M solution of CTAB under ultrasonication. A white turbid suspension forms initially but quickly redissolves. Then, 1.8 mL of an aqueous 0.1 M solution of SDS is added. Separately, 50.6 mg of 1,3,5-tris(4'-aminophenyl)benzene is dissolved in 0.25 mL of DMSO. This solution is added dropwise to 58 mL of an aqueous 0.1 M solution of CTAB under ultrasonication. A white turbid suspension forms initially but quickly redissolves. Then, 1.8 mL of an aqueous 0.1 M solution of SDS is added. Finally, the two resulting aqueous solutions are mixed and 5.8 mL of acetic acid added to the mixture. The solution is deoxygenated by performing 3 vacuum-argon cycles and allowed to react at 30ºC for 72 hours. A completely transparent orange colloidal solution is formed.

TAPB-BTCA COF(s) flocculation

In order to isolate the product in solid form, the reaction mixture is neutralized with 6.8 mL of concentrated ammonia and 100 mL of ethanol, yielding the formation of a yellow solid. The dispersion is centrifuged for 3 minutes at 1500 rcf and the supernatant removed. The solid is redispersed in 50 mL of ethanol and stirred for 30 minutes before centrifuging again. This washing procedure is repeated a total of 8 times, and a highly concentrated dispersion in ethanol is obtained. Finally, the sample is activated by critical point drying. 61.3 mg of a yellow powder is obtained (88 % yield). Elemental analysis: *Experimental*: C: 82.14 %, H: 5.04 %, N: 8.68 %. *Calculated for* $C_{33}H_{21}N_3 \cdot 1.25H_2O$: C: 82.24 %, H: 4.88 %, N: 8.72 %.

Synthesis of 20 nanometer **Tz-COF particles**

36.6 mg of benzene-1,3,5-tricarboxaldehyde is dissolved in 0.4 mL of DMSO. This solution is added dropwise to 90 mL of an aqueous 0.1 M solution of CTAB under ultrasonication. A white turbid suspension forms initially but quickly redissolves. Then, 2.78 mL of an aqueous 0.1 M solution of SDS are added. Separately, 80 mg of 2,4,6-tris(4'-aminophenyl)-1,3,5-triazine are dissolved in 0.4 mL of DMSO. This solution is added dropwise to 90 mL of an aqueous 0.1 M solution of CTAB under ultrasonication. A white turbid suspension forms initially but quickly redissolves. Then, 2.78 mL of an aqueous 0.1 M solution of SDS is added. Finally, the two resulting aqueous solutions are mixed and 9 mL of acetic acid added to the mixture. The solution is deoxygenated by performing 3 vacuum-argon cycles and allowed to react at 30 ºC for 5 days. A completely transparent yellow colloidal solution is formed.

Tz-COF(s) flocculation

In order to isolate the product in solid form, the reaction mixture is neutralized with 10 mL of concentrated ammonia and 100 mL of ethanol, with a yellow solid appearing. The dispersion is centrifuged for 3 minutes at 1500 rcf and the supernatant is removed. The solid is redispersed in 50 mL of ethanol and stirred for 30 minutes before centrifugation. This washing procedure is repeated a total of 8 times, yielding a highly concentrated dispersion in ethanol. Finally, the sample is activated by critical point drying. 104 mg of a yellow powder is obtained (93 % yield). Elemental analysis: *Experimental*: C: 72.72 %, H: 4.33 %, N: 16.89 %. *Calculated for* $C_{30}H_{18}N_6 \cdot 1.75H_2O$: C: 72.95 %, H, 4.36 %, N: 17.02 %.

Synthesis of 20 nanometer **MIL-100(Fe)** particles

40.2 mg of sodium hydroxide is dissolved in 61 mL of an aqueous 0.1 M solution of SDS. Subsequently 70.47 mg of trimesic acid is added and ultrasonicated until the solid is completely dissolved. Then, 2 mL of an aqueous 0.1 M solution of CTAB is added. Separately, 100 mg of $FeCl_2 \cdot 4H_2O$ is dissolved in 42 mL of an aqueous 0.1M solution of SDS. Next, 1 ml of an aqueous 0.1 M solution of CTAB is added. Finally, the trimesic acid solution is added over the stirred solution of $FeCl_2 \cdot 4H_2O$ dropwise. Stirring is stopped and the resulting solution allowed to react at 30 ºC for 48 hours, yielding a completely transparent orange suspension. In order to isolate the product in its solid form, 100 ml of ethanol is added to the reaction mixture. The dispersion is centrifuged for 4 minutes at 6300 rcf and the supernatant removed. The orange solid is redispersed in 50 ml of ethanol and stirred for 30 minutes before centrifugation. This washing step is repeated a total of 3 times. Finally, the sample is activated by critical point drying. 75 mg of an orange powder is obtained (86 % yield).

Synthesis of millimeter **TAPB-BTCA COF(s)** films

First, a polydimethylsiloxane (PDMS) pre-polymer and curing agent (SYLGRAD 184, DOW Silicones Deutschland GMBH) mixture was prepared using a 10:1 ratio in weight, respectively. The mixture was kept under vacuum for 30 minutes to allow degassing. Next, a commercial microscope glass slide (26 mm x 76 mm, Thermo Scientific TM Frosted, Fisher Scientific Ltd., Finland) was spin-coated at 500 rpm for 10 seconds and at 1200 rpm for 50 seconds in two consecutive steps with the mixture of degassed PDMS elastomer and curing agent to yield a 50 µm PDMS layer over the glass slide. Then the glass slide was placed in an oven at 70 ºC and cured for 8 hours. After the curing step, a rectangular piece of PDMS was cut and removed from the slide to obtain a confined space. A second glass slide was then clamped to the PDMS structured glass slide. Subsequently, the concentrated reaction mixture was poured between the two glass slides into the gap, and the whole system clamped. Finally, residual ethanol was evaporated to form the **TAPB-BTCA COF(s)** film.

Synthesis of micrometer **TAPB-BTCA COF(s)** films

The concentrated reaction mixture was placed between a machined stainless-steel stamp containing 500 µm by 500 µm square holes and a glass slide covered with filter paper. The absorption of the ethanol by the filter paper facilitated the formation of 500 µm by 500 µm **TAPB-BTCA COF**(s) films.

Synthesis of **TAPB-BTCA COF(s)** octahedra

First, the designed mold for the octahedral shapes was manufactured with a 3D printer (ProJet MJP 2500/2500 Plus, 3D systems, U.S.). Next, the concentrated **TAPB-BTCA COF** colloid was injected into the mold. Subsequently, the mold was introduced in a CO_2 critical point dryer chamber and the **TAPB-BTCA COF** octahedra were obtained.

Fabrication of microfluidic device used for the direct printing of **TAPB-BTCA COF(s)**

To fabricate the concentric 3D focusing device, a negative mold was first fabricated by inserting a commercial syringe needle (OD: 0.5 mm, cut length: 2 cm) inside a 5 cm long polytetrafluoroethylene (PTFE) tubing (OD: 1mm, 0.5 mm). A PDMS pre-polymer and curing agent (SYLGRAD 184, DOW Silicones Deutschland GMBH) mixture was prepared using a 10:1 ratio in weight, respectively, and kept under vacuum for 30 minutes to degas the mixture. Then,

the negative mold of the channel was immersed in the PDMS elastomer and curing agent mixture, whilst ensuring that the mixture does not penetrate the needle and PTFE tube. After curing in an oven at 70ºC for 8 hours, the PDMS slab was cut with a razor blade and the sacrificial PTFE tubing was removed to form the main channel. The needle was kept inserted in the cured PDMS slab to form the concentric inlet for the central stream. To introduce the concentric sheath flow, that wraps the central stream, a 1 mm hole was formed with a biopsy punch (Miltex GmbH) in the top part of PDMS, at the middle point of the needle.

Direct printing of **TAPB-BTCA COF(s)**

Initially, the reaction mixture was concentrated by evaporation to half volume. This solution was then injected through the central inlet at a flow rate of 100 μL min^{-1} (**Figure 3D**). Ethanol was pumped at 50 μL min^{-1} through the other inlet. The outlet tubing of the device was kept at 70ºC and used to directly print **TAPB-BTCA COF(s)** onto glass slides.

Particle models used for the analysis and fitting of SAXS data

The SAXS profiles at short reaction times (5h) were fitted using a simple disk model consisting of bare **TAPB-BTCA COF** single layer (see Fig. S13A). In order to fix some parameters for the fitting, the radius of the disc was calculated from the DLS data using the relation between the hydrodynamic radius and the equivalent radius for an ellipsoid:

$$\frac{R_H}{R_S} = \frac{\left(1-p^2\right)^{1/2}}{p^{2/3}\ln\left[\frac{1+\left(1-p^2\right)^{1/2}}{p}\right]} \qquad \text{(Equation 1)}$$

Here R_H is the hydrodynamic radius, R_S is the radius of the equivalent sphere and p is the ratio of the major axis to the minor axis of an ellipsoid.[11] Using the calculated radius of 6.4 nm and 0.354 nm as the thickness expected for a single layer of **TAPB-BTCA COF**, intensity was used as the single parameter to fit the spectra (**Table S1**). The electron density of **TAPB-BTCA COF** needed for the calculation was estimated to be 427 e/nm^3, a value that considers the pores to be completely full with water, with a content based on the volume of the crystalline cell minus the Van der Waals volume of the COF.

At 13 and 21 hours SAXS profiles show a significantly increased intensity at low values of the scattering vector (q < 1 nm^{-1}) along with the appearance of intense features at q > 1 nm^{-1}, the latter suggesting changes in electronic contrast.[7] It should be noted that the use of the previous model does not allow fitting, even when all parameters are free. Accordingly, a model that considers the **TAPB-BTCA COF** particle to be surrounded by a layer of surfactant molecules was considered, i.e. a core-two-shells model (COF-core@double-shell)(**Fig. S13B**), comprising a core with low electron density (**TAPB-BTCA COF**), an inner shell with hydrocarbon electron density (the hydrophobic chains of the surfactant) and an outer shell of high electron density (the hydrated polar head groups of the surfactants). In this case, the thickness and electron density of the core together with the thickness of the hydrophobic and hydrophilic layers were used as fitting parameters, while the particle radius as calculated from the DLS data (**Table S1**) is kept constant. It should also be noted that the surfactant layer provides a hydrophobic environment surrounding the stacks of **TAPB-BTCA COF**. Thus the water content in the pores of the COF is expected to be lower than in the case of bare **TAPB-BTCA COF** disks, which results in a diminished electron density of the core.

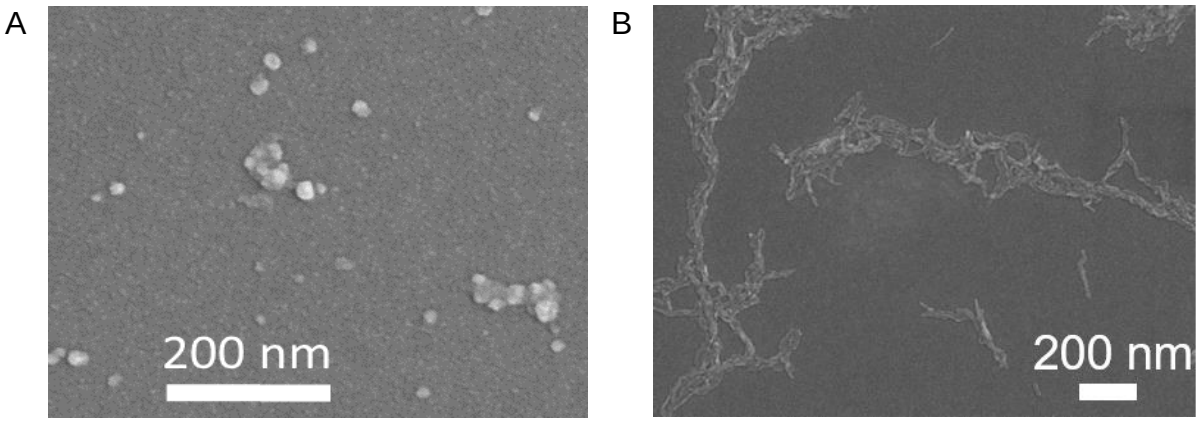

Fig. S1.

SEM images of drop-cast **TAPB-BTCA COF** nanoparticles formed by using the *catanionic* micellar system CTAB/SDS at surfactant ratio **(A)** CTAB/SDS 97:3 and **(B)** CTAB/SDS 85:15 respectively.

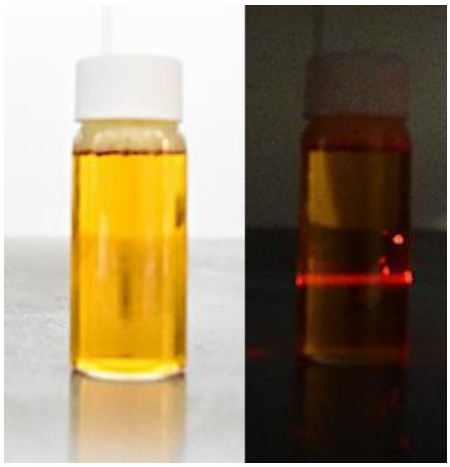

Fig. S2.
Photograph of a transparent and homogeneous **TAPB-BTCA COF** colloidal solution (left), with the same sample showing the Tyndall effect upon irradiation with laser light at 630 nm (right).

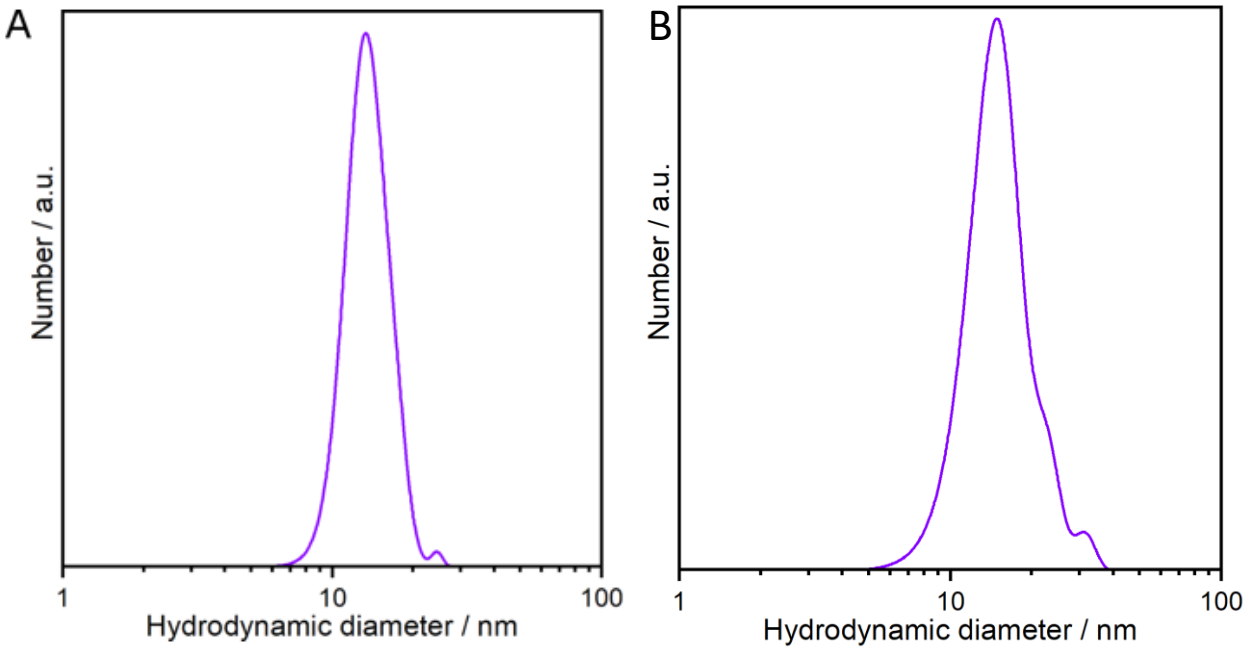

Fig. S3.

Size distributions obtained by DLS of the **TAPB-BTCA COF** colloidal solution after (**A**) 24 hours and (**B**) six months, demonstrating that the size distribution does not change appreciably at long times.

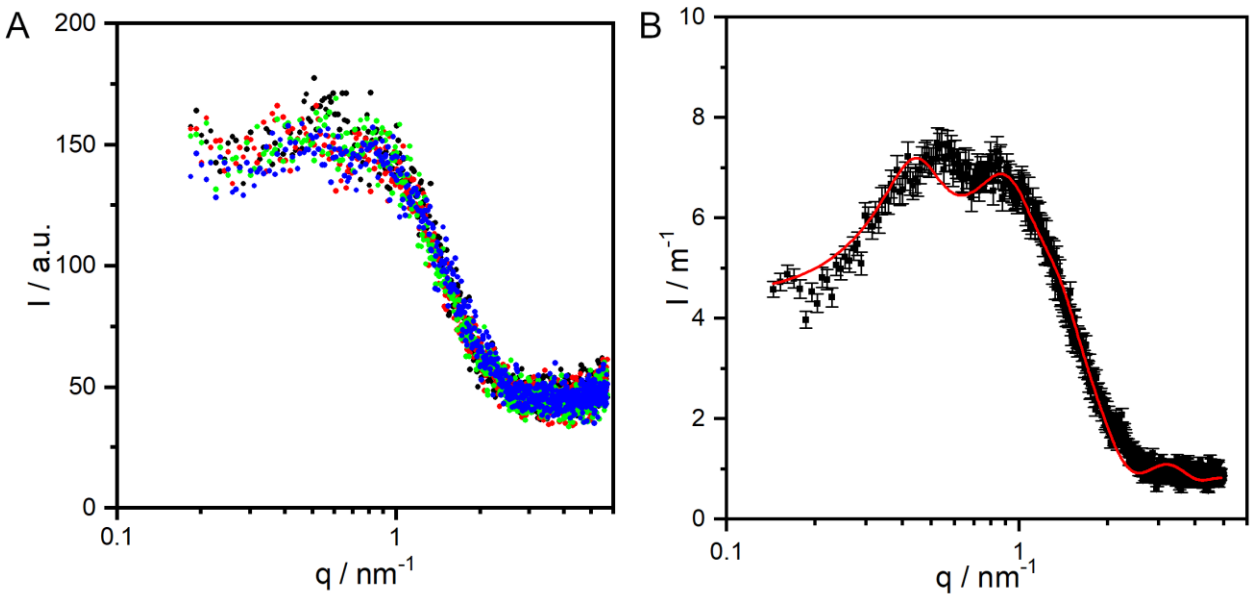

Fig. S4.

(**A**) SAXS profiles of aqueous solutions of CTAB/SDS 97/3 (red), CTAB/SDS 97/3 with 5 % volume acetic acid (black), **BTCA** in CTAB/SDS 97/3 (green) and **TAPB** in CTAB/SDS 97/3 (blue). No significant statistical differences are observed. (**B**) Fitting of the data in (**A**), after water background subtraction, to the ellipsoidal model used to calculate the size of the CTAB/SDS mixed micelles prior to the reaction.

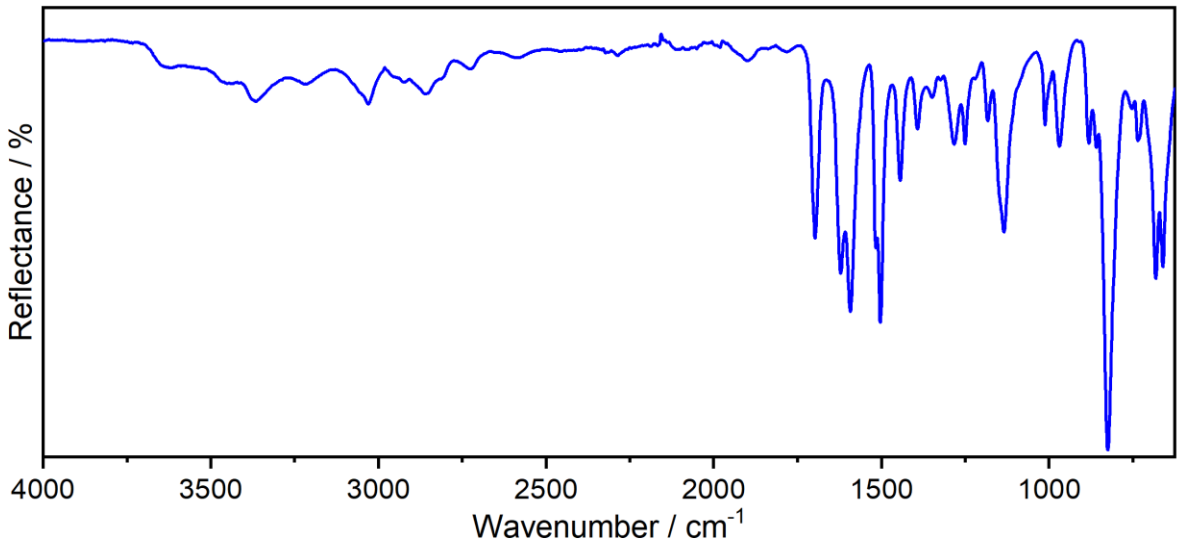

Fig. S5.

ATR-FT-IR spectrum of **TAPB-BTCA COF(s)** after critical point activation. The spectrum agrees well with spectra reported for COFs with this structure.[1] The band at 1622 cm^{-1} corresponds to the C=N stretch of the imine bond. It should be noted that the residual bands of the C-O stretch of the aldehyde (1698 cm^{-1}) and the N-H stretches of the amines (3452, 3367, 3216 cm^{-1}) are stronger than observed in the literature due to the large number of unreacted groups at the edges of the nanoparticles.

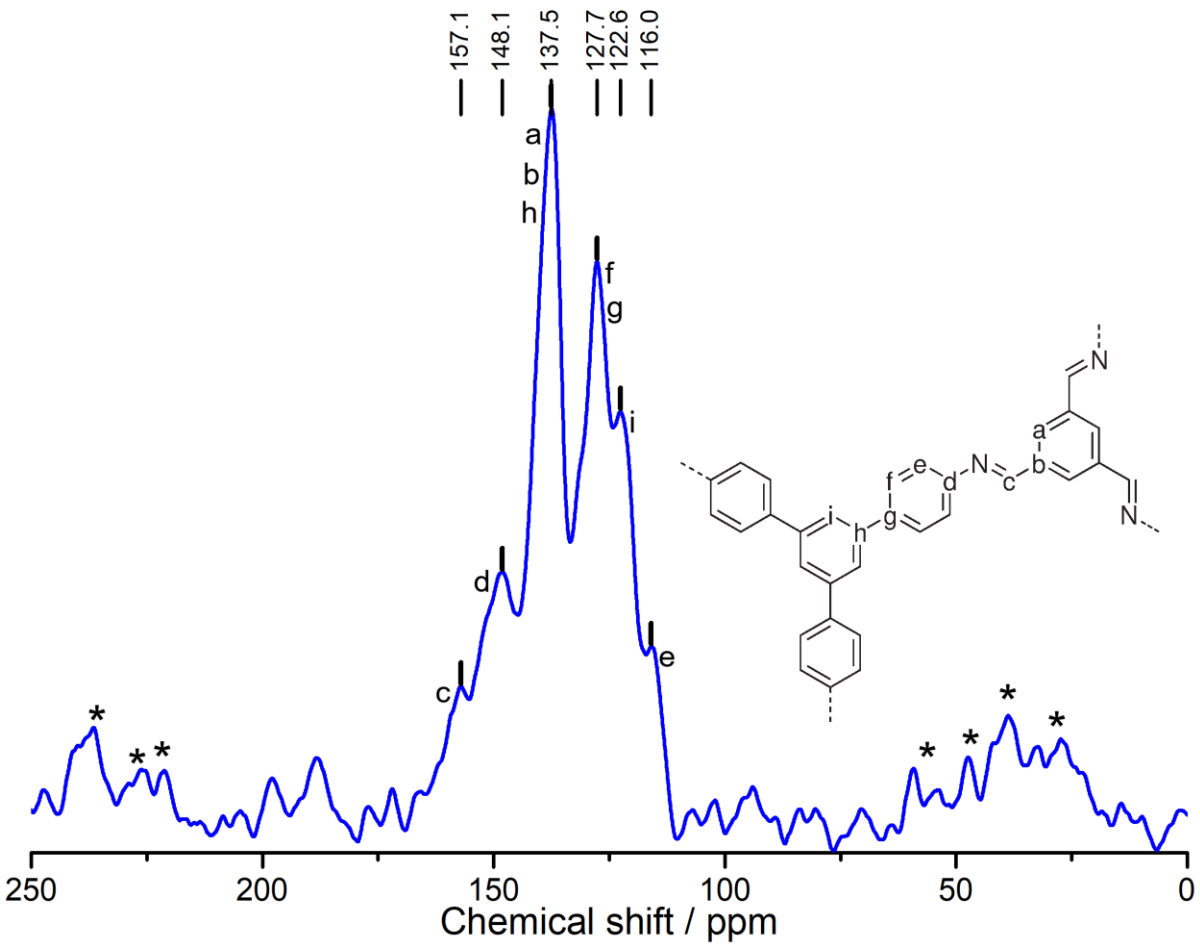

Fig. S6.

^{13}C CP-MAS NMR spectrum of **TAPB-BTCA COF(s)**. The signal assignments are displayed on the fragment of the structure. Asterisks denote spinning sidebands.

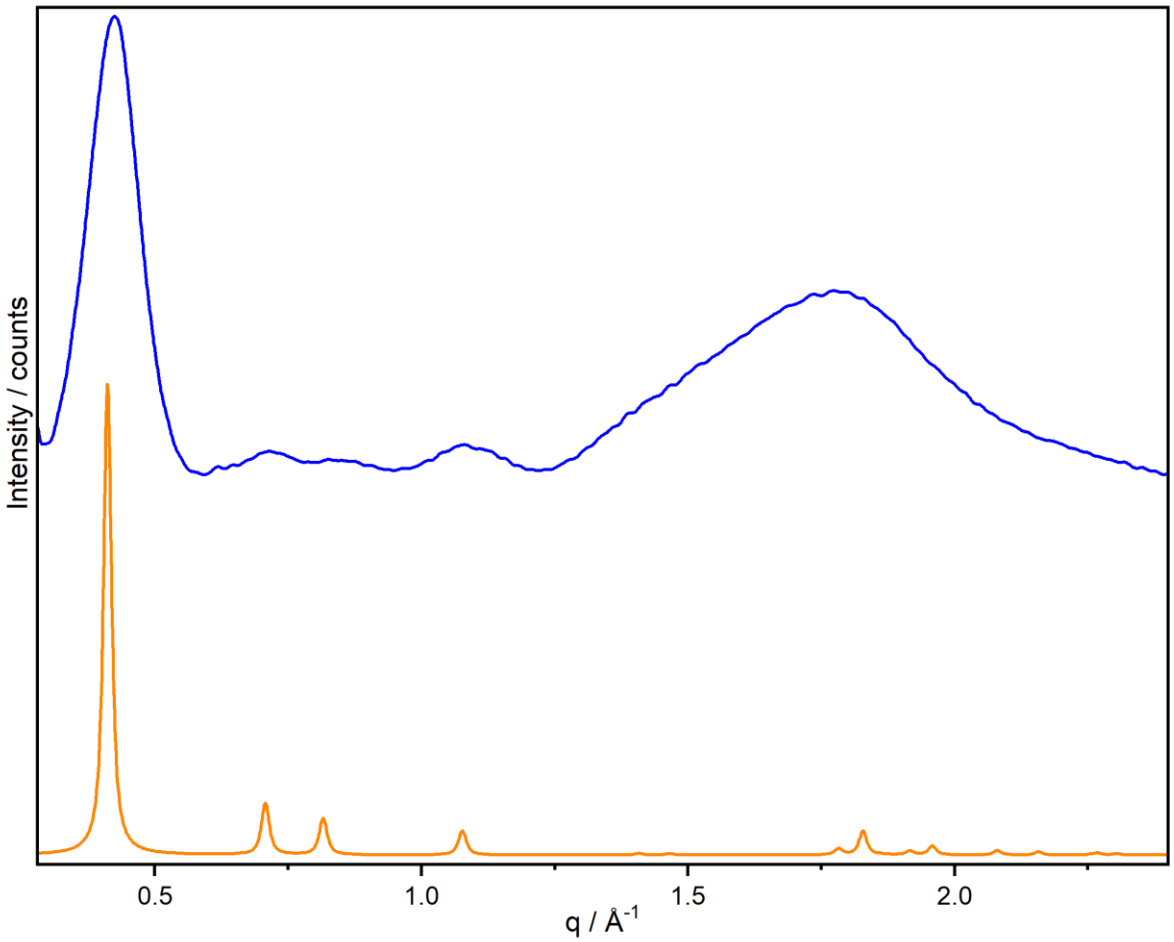

Fig. S7.

Experimental (blue) and simulated (orange) PXRD patterns of **TAPB-BTCA COF(s)** after critical point drying. Data for the calculation of the theoretical pattern were obtained from reference.[1]

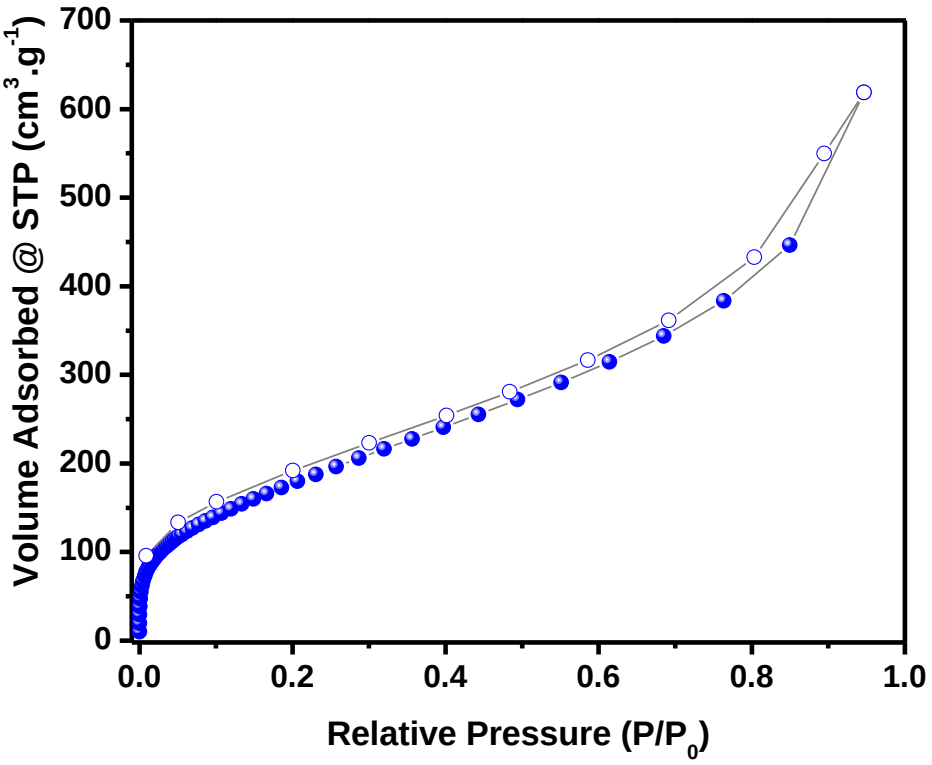

Fig. S8.

N_2 adsorption (solid dots) and desorption (open dots) isotherms of **TAPB-BTCA COF(s)**. A fit to the BET model yields a surface area of 687 m^2/g at 77 K.

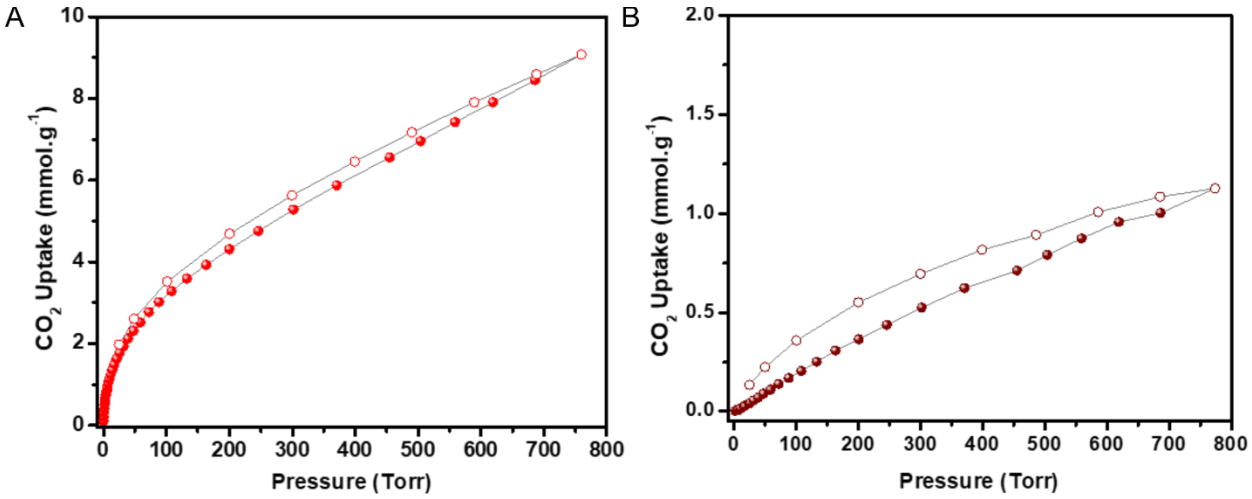

Fig. S9.

CO_2 adsorption (solid dots) and desorption (open dots) isotherms of **TAPB-BTCA COF(s)** at a) 203 K and b) 298 K.

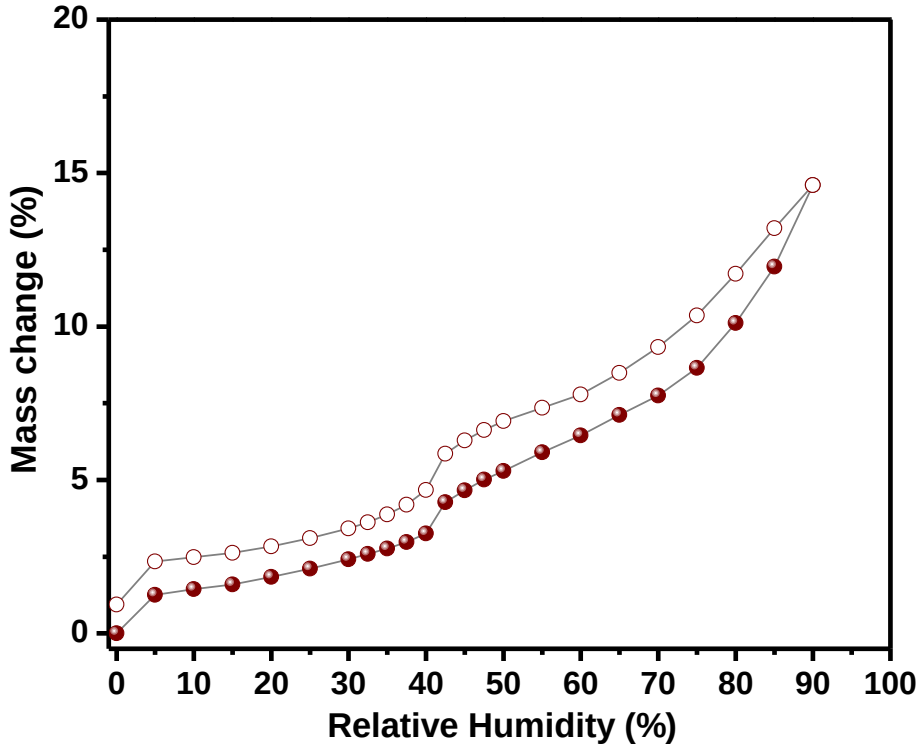

Fig. S10.
Water sorption (solid dots) and desorption (open dots) isotherms of **TAPB-BTCA COF(s)** at 298 K.

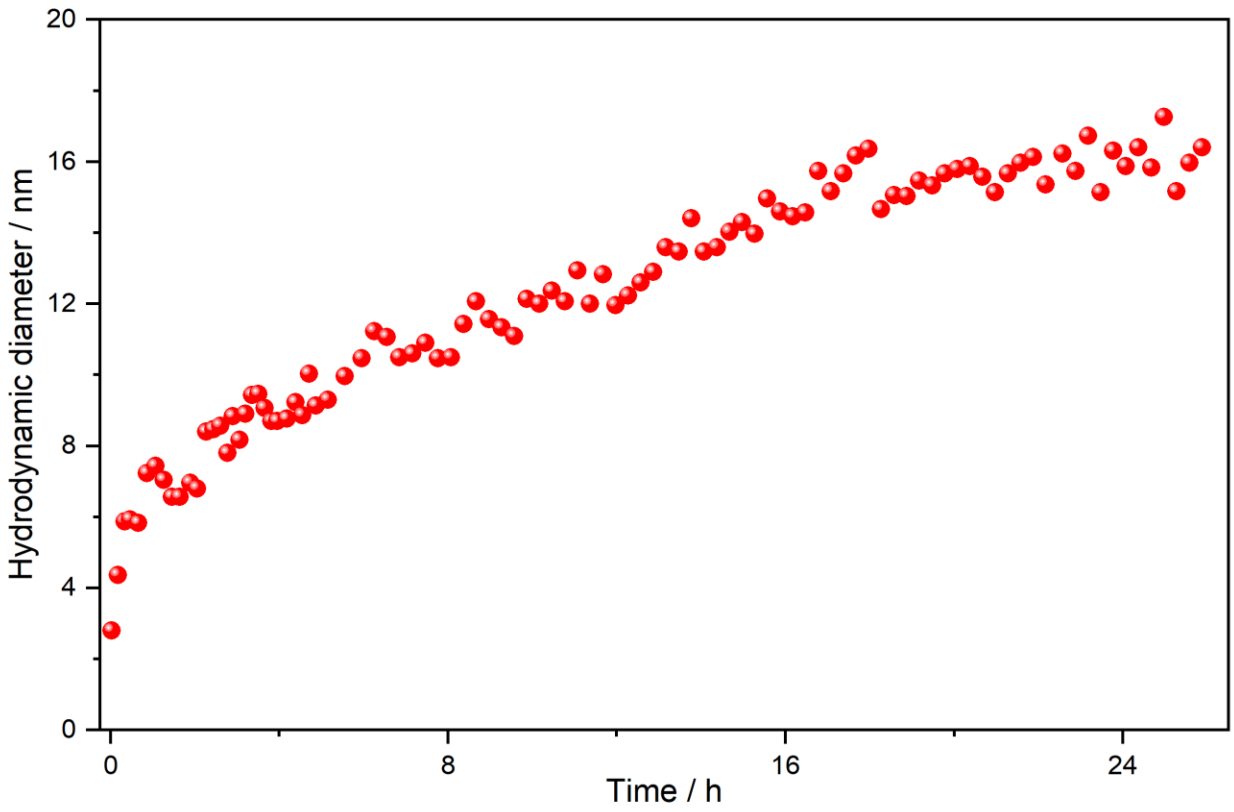

Fig. S11.
Variation in hydrodynamic diameter of the **TAPB-BTCA COF** reaction mixture as a function of time during the first 26 hours of reaction.

CTAB/SDS molar ratio	COF nanoparticle hydrodynamic diameter (nm)
100:0	15
99:1	15
97:3	16
95:5	18
93:7	73

Table S1.

Average hydrodynamic diameter of **TAPB-BTCA COF** nanoparticles measured by DLS after 24 hours of reaction.

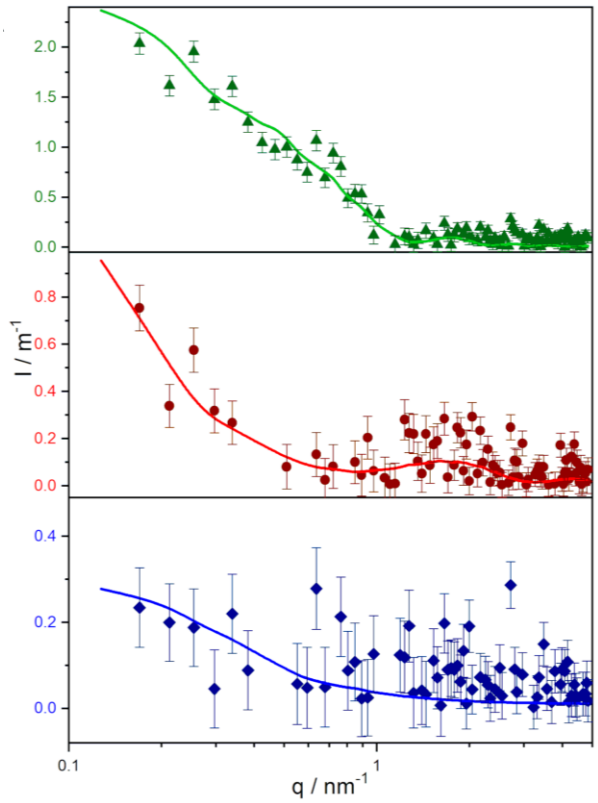

Fig. S12.

SAXS profiles at different time points during reaction (symbols) with corresponding fits to the used model (lines). Low intensities are recorded at 5 hours (blue), with a completely flat curve at high values of the scattering vector (q > 1 nm^{-1}). As the reaction proceeds, the intensity at low q values (below 1 nm^{-1}) clearly increases, with a peak appearing at 2 nm^{-1} at 13 hours (red). Further enhancement of this feature is seen at 21 hours (green).

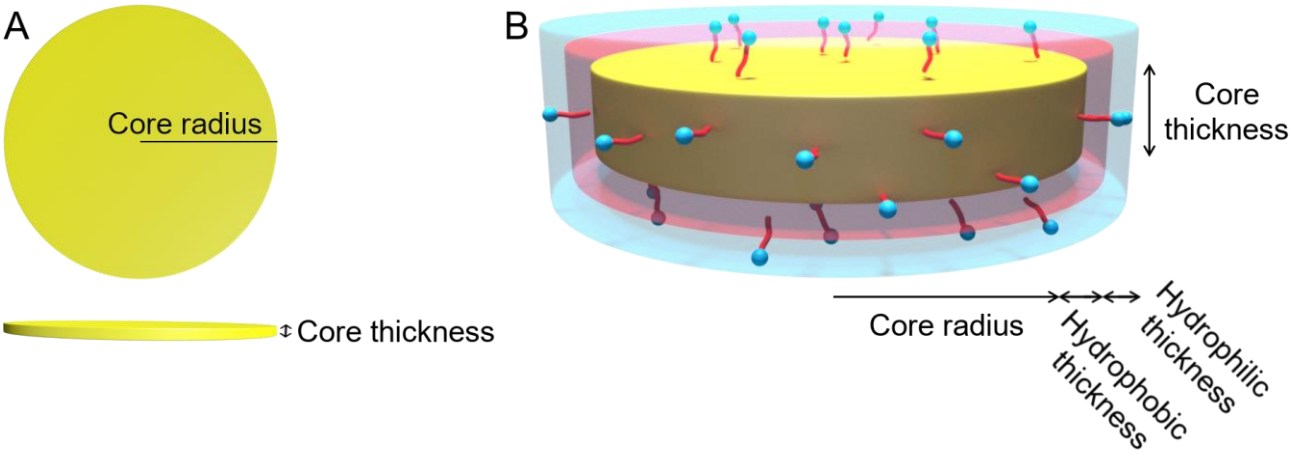

Fig. S13.

(**A**) Schematic describing the model used for fitting SAXS profiles at short times, illustrates a bare **TAPB-BTCA COF** disk a single layer thick. (**B**) Schematic describing the model used to fit SAXS profiles at longer reaction times, illustrating a disk with a **TAPB-BTCA COF** core, an inner shell composed of the hydrophobic tails of the surfactants and an outer shell comprising the polar heads. The parameters presented in **Table S1** are indicated.

Time (h)	**5**	**13**	**21**
Model used	Disk model	COF-core@double-shell	
Core radius (nm)[1]	6.4±0.2	7.9±0.3	8.9±0.2
Core thickness (nm)	0.354 [2]	0.91±0.08	3.74±0.15
Core electron density (e nm^{-3})	427 [2]	322±8	284±8
Hydrophobic thickness (nm)	-	0.72±0.05	0.93±0.05
Hydrophobic layer electron density (e nm^{-3})	-	300 [2]	300 [2]
Hydrophilic thickness (nm)	-	0.39±0.05	0.47±0.05
Hydrophilic layer electron density (e nm^{-3})	-	436±8	439±8
Intensity scale	0.93±0.05	1 [2]	1 [2]
Reduced *chi-squared*	1.7	1.9	2.4

Table S2.

Parameters used for fitting SAXS profiles of **TAPB-BTCA COF** nanoparticles at 5, 13 and 21 hours. Hydrophobic thickness and hydrophilic thickness refer to the thickness of the aliphatic and polar regions of the surfactant surrounding the COF (see the schematic model in Fig. S13). [1] Parameter calculated from DLS data and Equation 1. [2] Parameters fixed for the fitting.

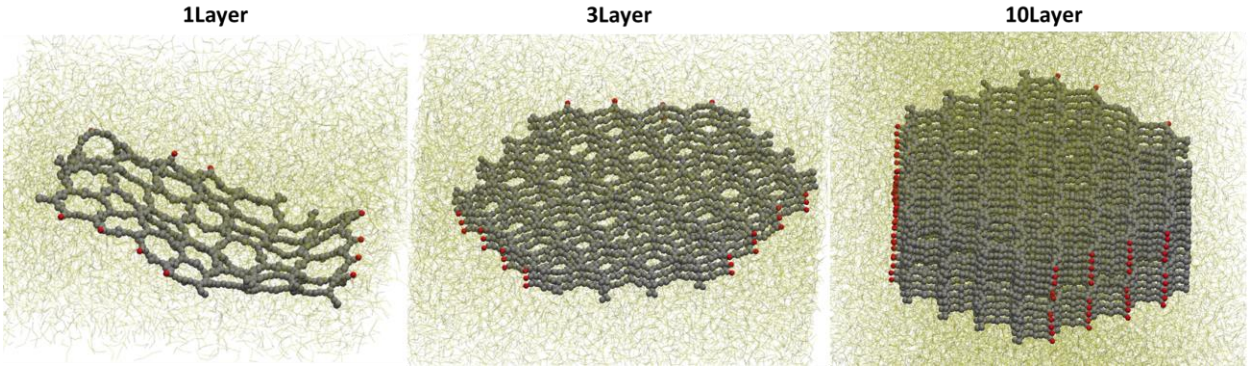

Fig. S14

Snapshots of **TAPB-BTCA COF** assemblies of 1, 3 and 10 layers, respectively, after CG-MD simulation in hexadecane. The hexadecane box mimics the hydrophobic environment of the micellar interior. Even in this environment, the COF layers prefer to aggregate.

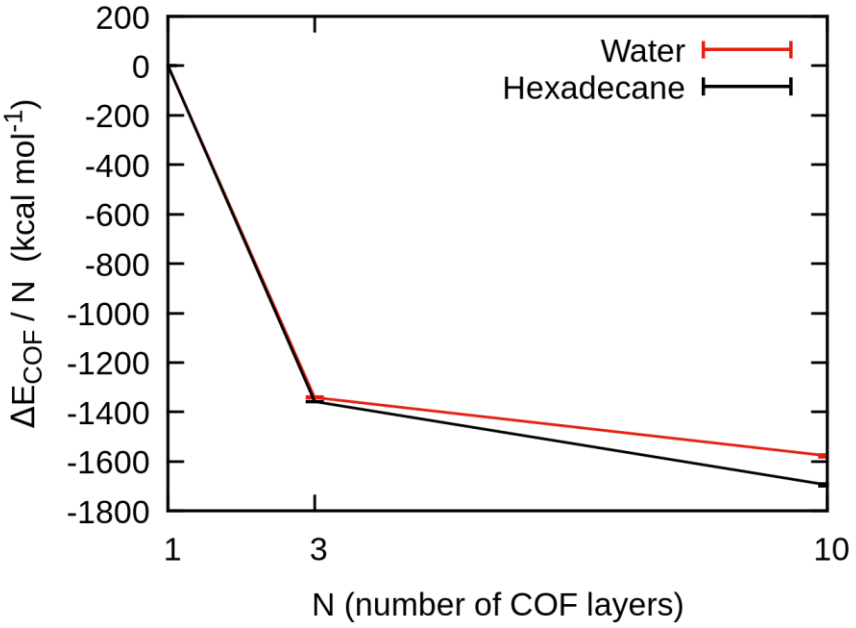

Fig. S15.

Solute-solute interaction energy between the COF layers normalized per-COF layer. Energy of a single layer is set to 0 as reference in the plot. The solute-solute interaction energy between the COF layers becomes more and more favorable while the number of layers in the COF stacking increases (3 vs. 10 layers), that is an evidence of cooperativity.

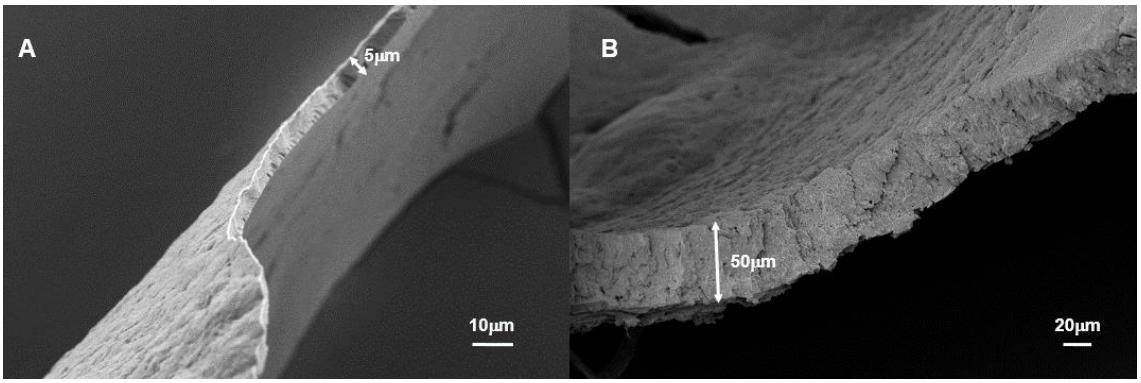

Fig. S16.

(A and B) SEM micrographs of the cross-section of **TAPB-BTCA COF(s)** films with different thickness.

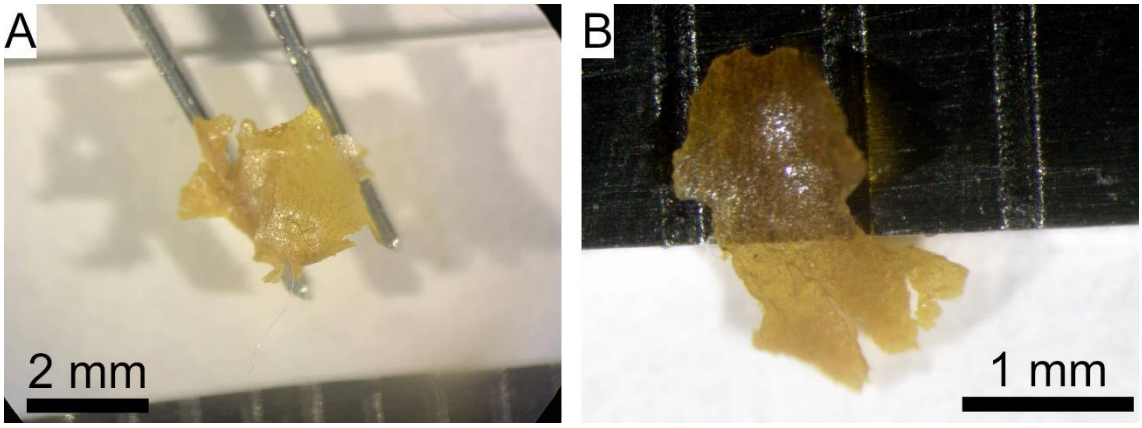

Fig. S17.
(A and B) Optical micrographs showing millimeter-sized freestanding **TAPB-BTCA COF(s)** films.

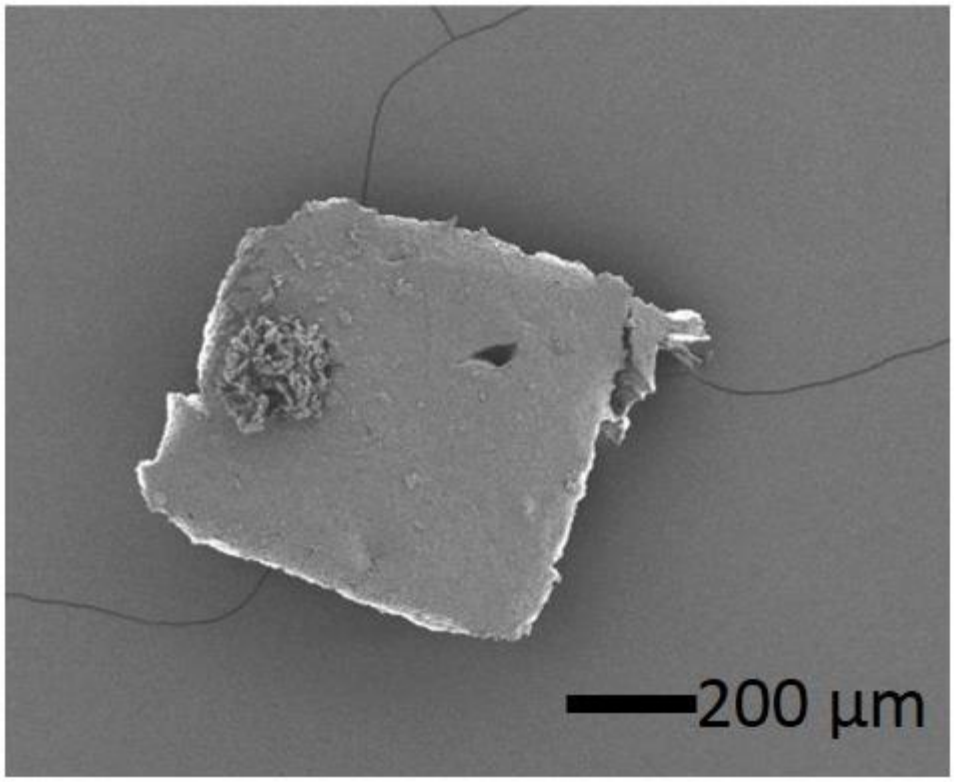

Fig. S18.
SEM micrograph of a **TAPB-BTCA COF(s)** film having a lateral size of approximately 500 µm.

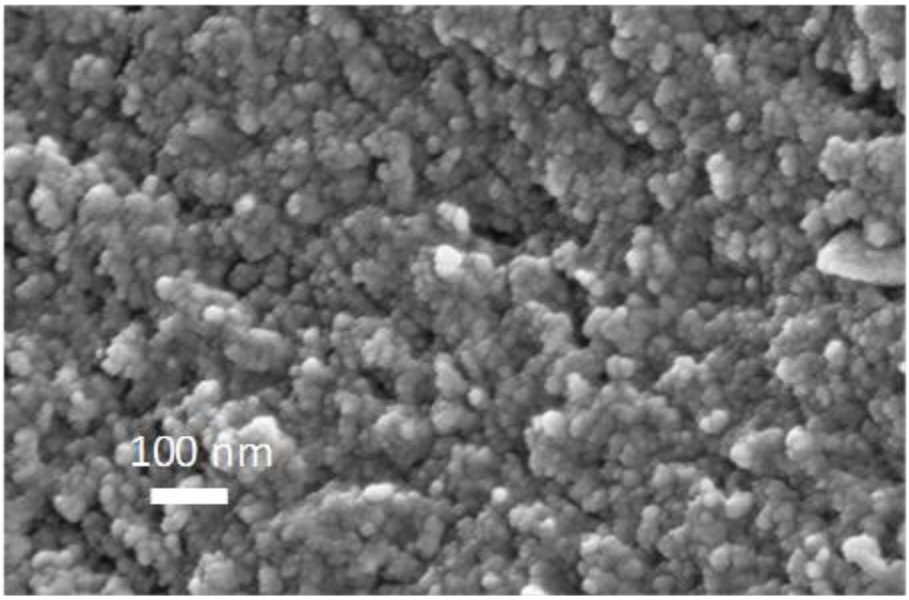

Fig. S19.
SEM image at high magnification of a **TAPB-BTCA COF(s)** film, highlighting its nanoparticulate texture.

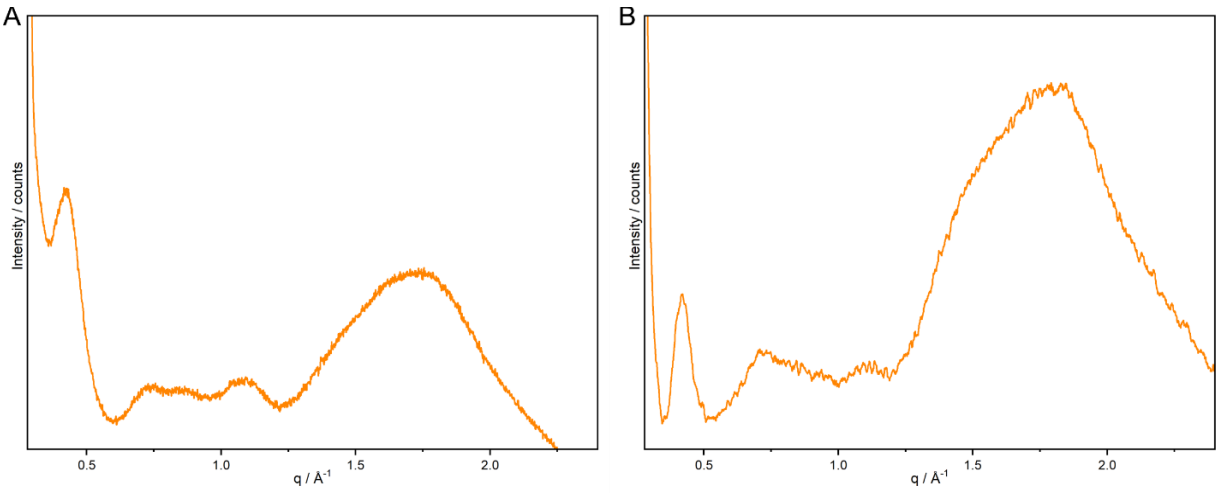

Fig. S20.

Experimental PXRD patterns of **TAPB-BTCA COF(s)** processed as (**A**) thin film, and (**B**) directly printed structures.

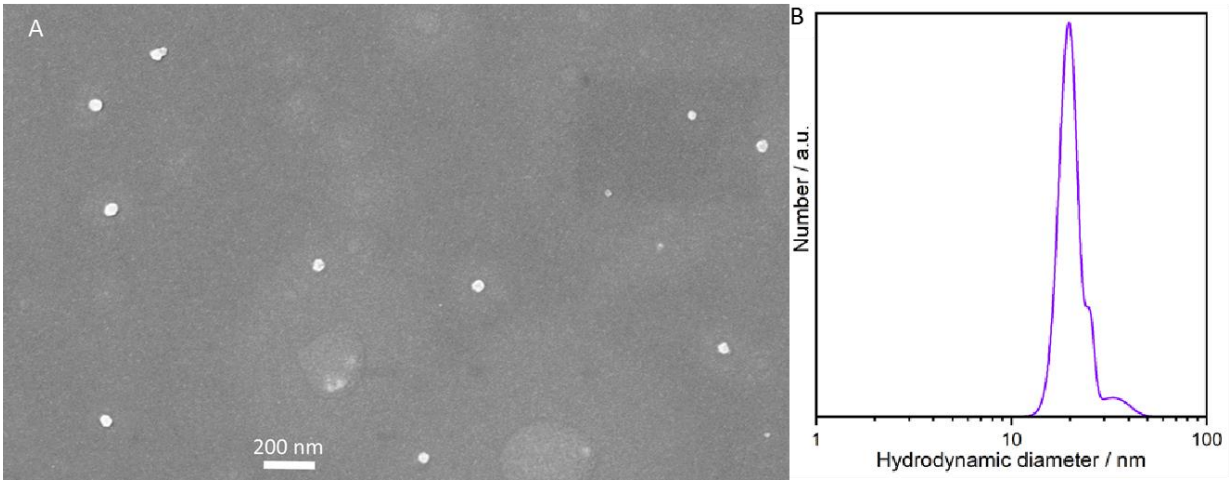

Fig. S21.

(**A**) SEM image of drop-cast **Tz-COF** nanoparticles. (**B**) Size distribution obtained by DLS from a colloidal solution of **Tz-COF**.

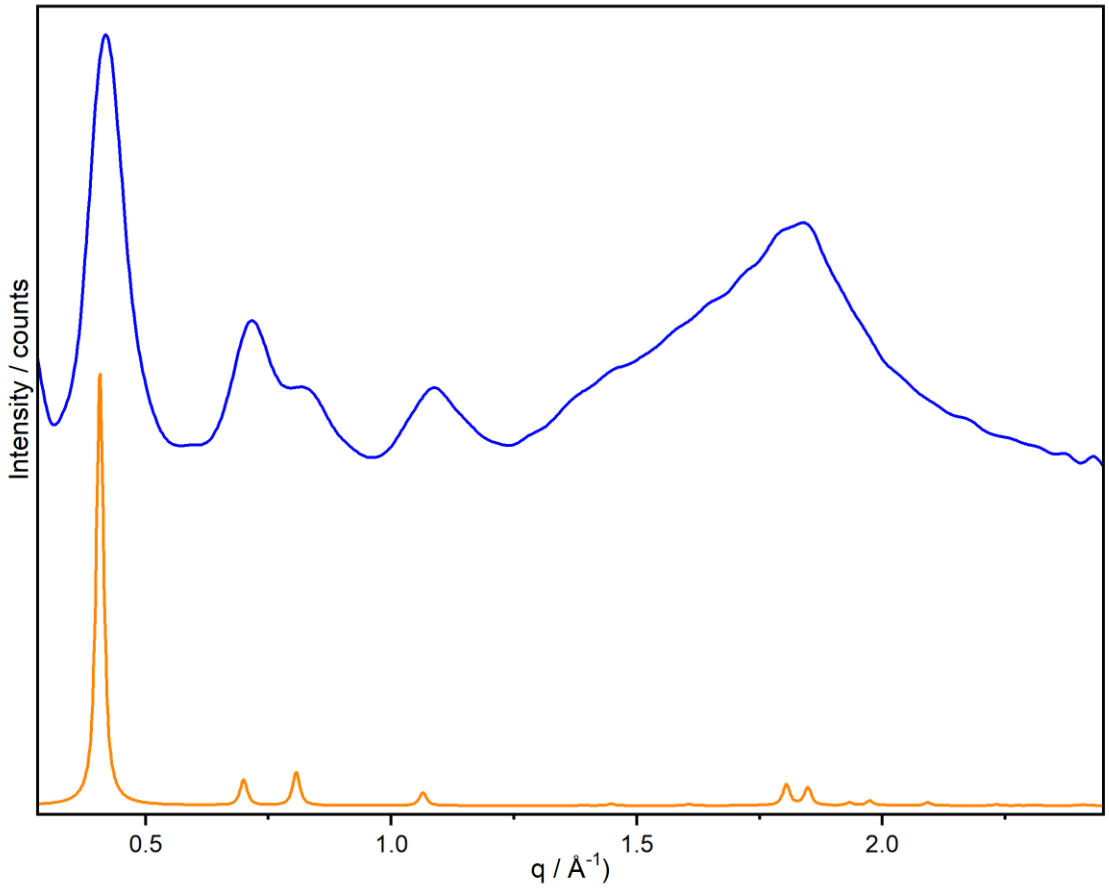

Fig. S22.
Experimental (blue) and simulated (orange) PXRD patterns of **Tz-COF** after critical point drying. Data for the calculation of the theoretical pattern were extracted from reference.[12]

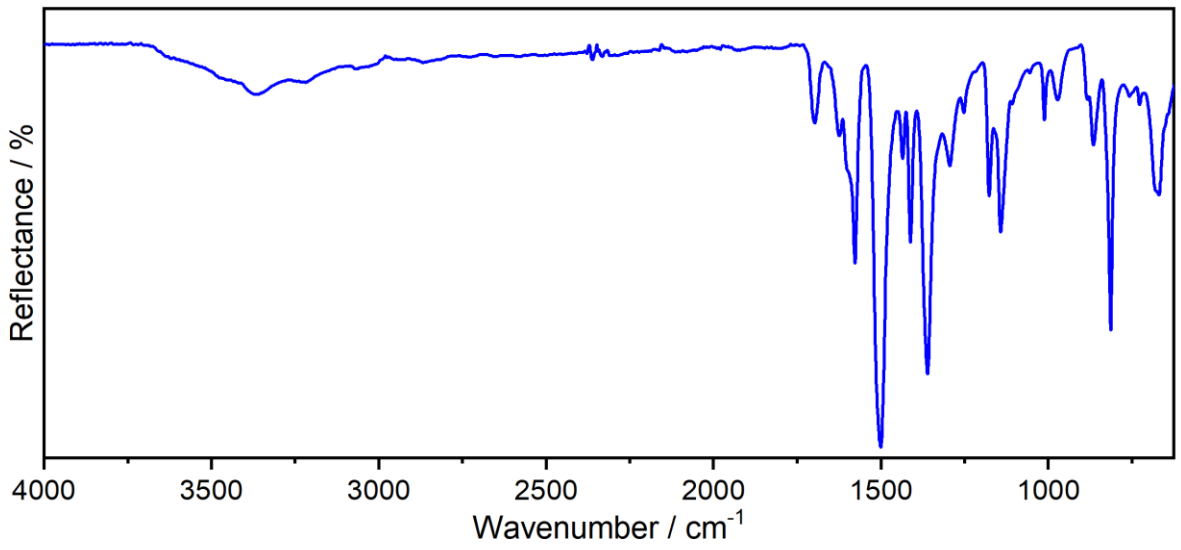

Fig. S23.

ATR-FT-IR spectrum of **Tz-COF** after critical point activation. The spectrum is almost identical to previously reported spectra for this COF.[13] The band at 1625 cm^{-1} corresponds to the C=N imine bond stretch, whilst the residual bands of the C-O stretch of the aldehyde (1697 cm^{-1}) and of the N-H stretch of the amines (3459, 3318, 3207 cm^{-1}) are stronger than previously reported due to the large number of unreacted groups at the edges of the nanoparticles.

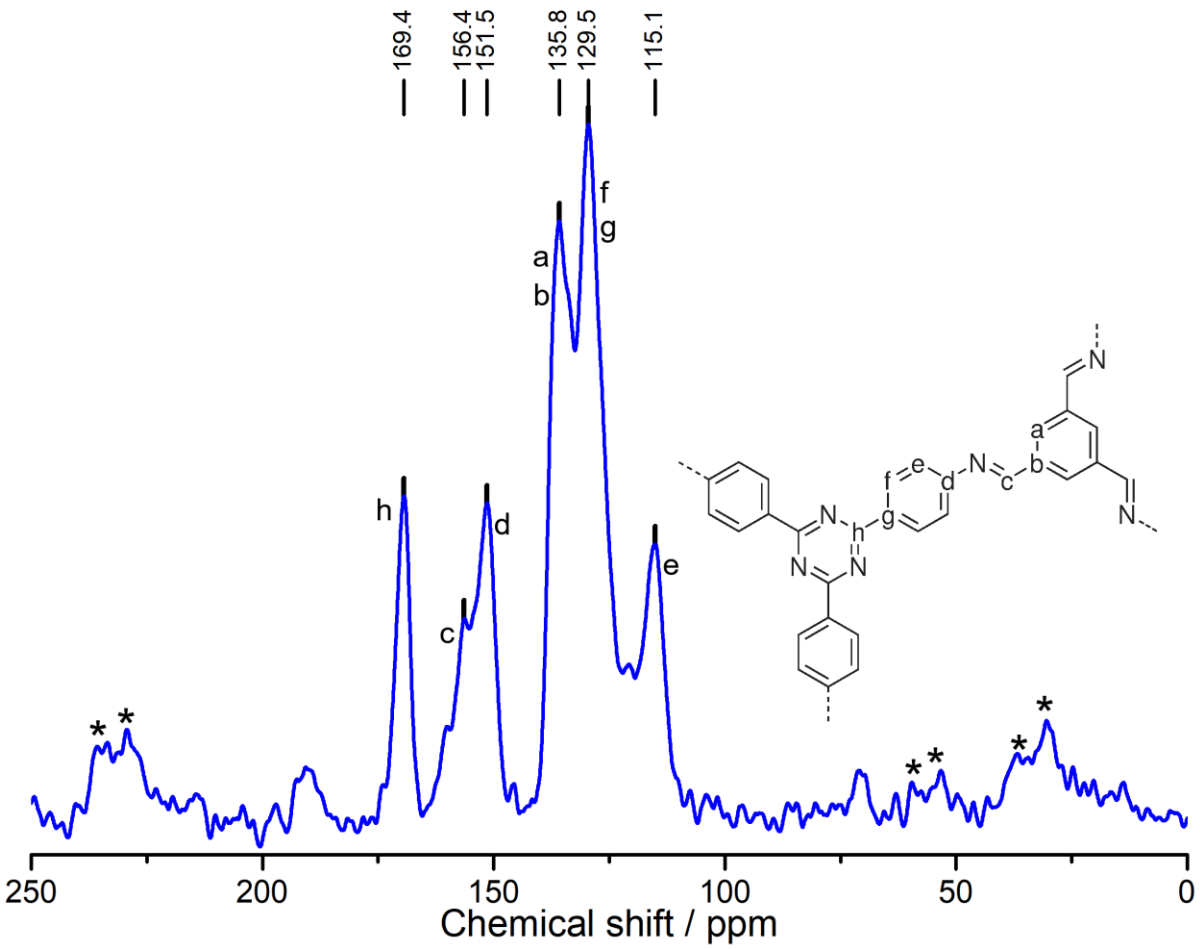

Fig. S24.

^{13}C-NMR spectrum of **Tz-COF**. The signal assignments are displayed on the fragment of the structure. Asterisks denote spinning sidebands.

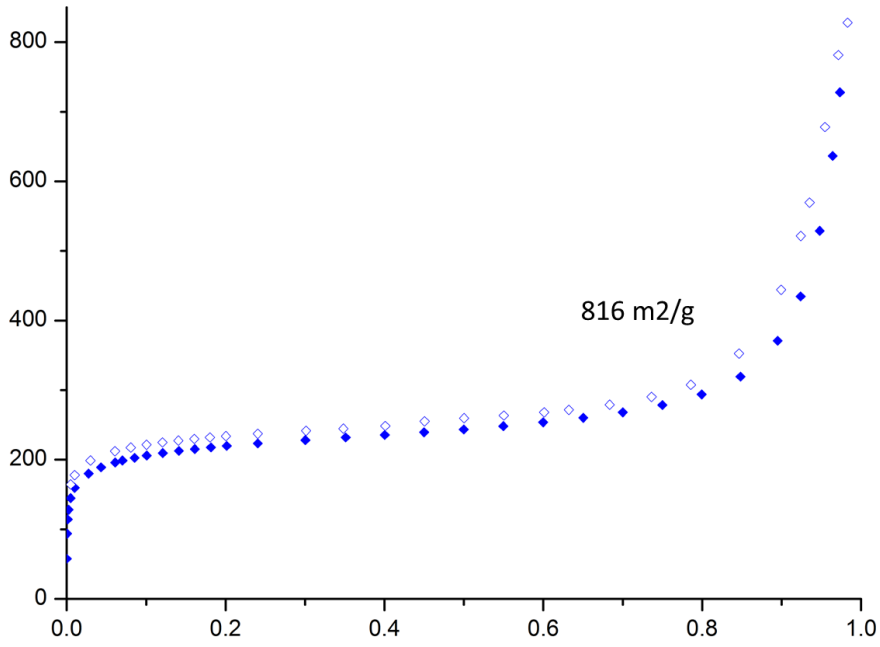

Fig. S25.

N_2 adsorption (solid dots) and desorption (open dots) isotherms of **Tz-COF** at 77K. Fits to the BET model yield a surface area of 816 m^2/g.

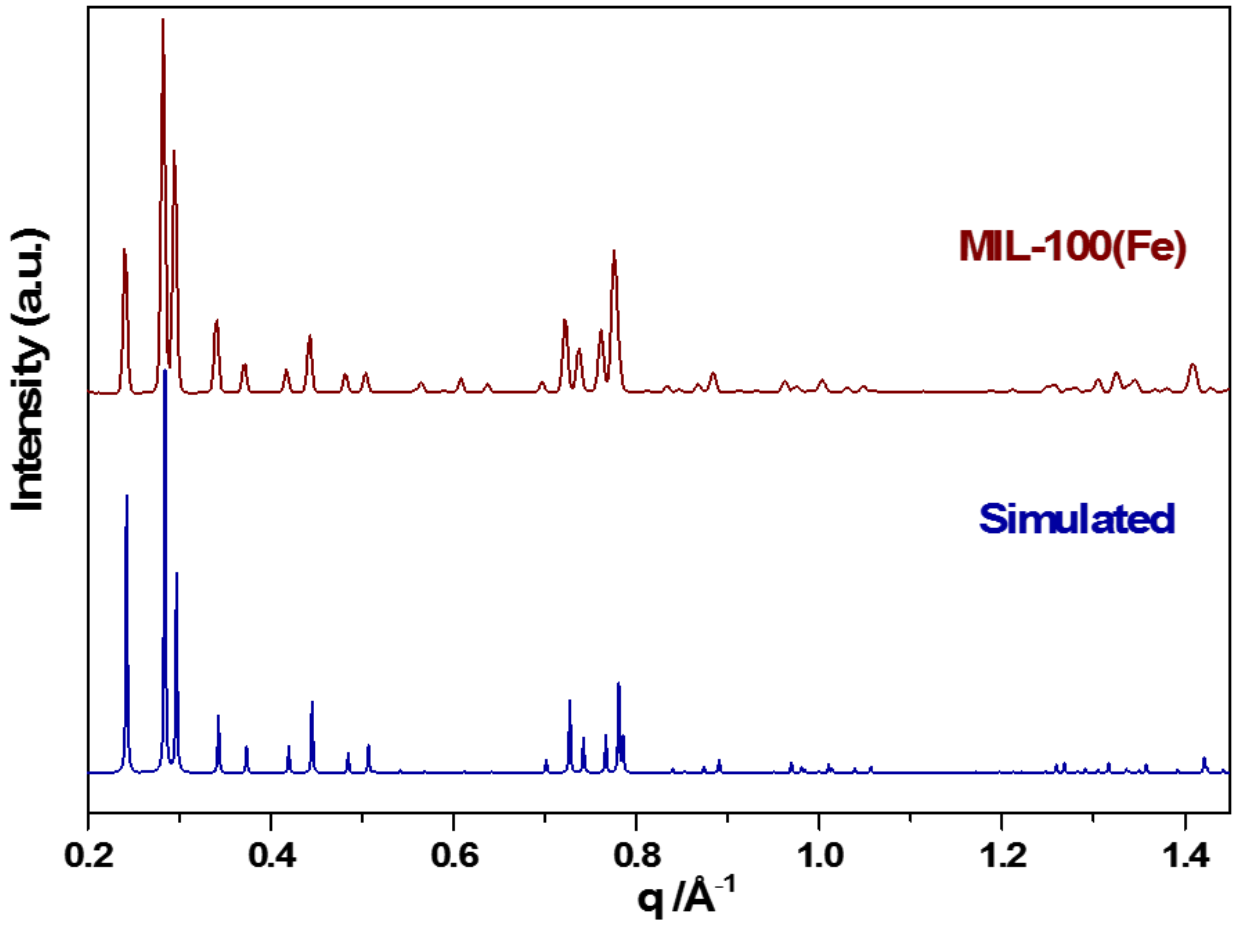

Fig. S26.

Experimental (red) and simulated (blue) XRD patterns of a **MIL-100(Fe)** colloidal solution obtained using synchrotron radiation. Data for the calculation of the theoretical pattern were obtained from reference.[14]

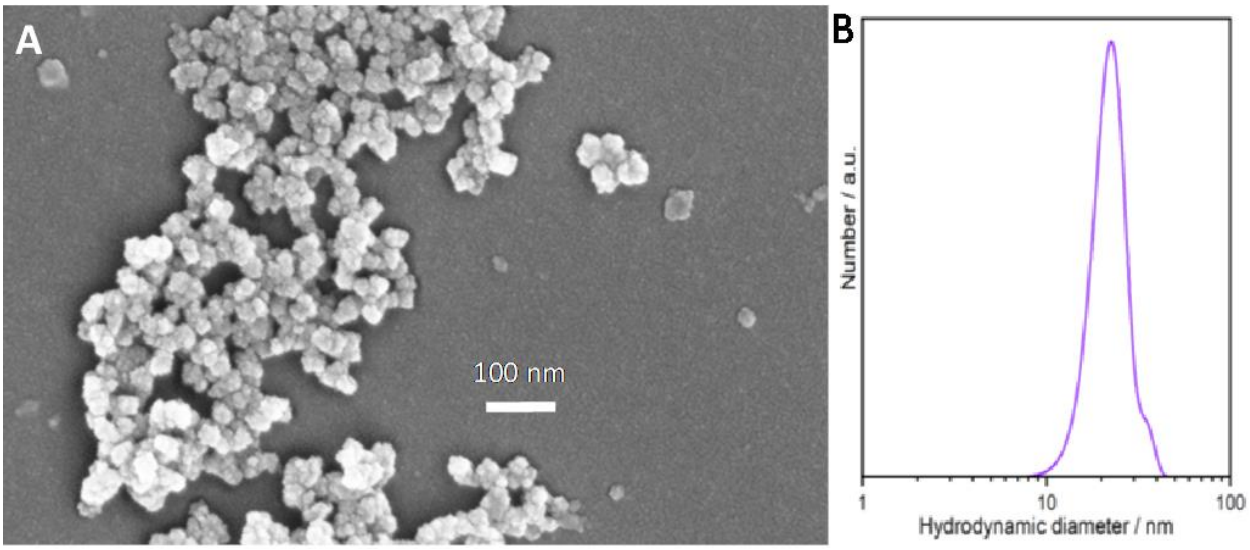

Fig. S27

(**A**) SEM images of drop-cast **MIL-100(Fe)** nanoparticles. (**B**) Size distribution obtained by DLS analysis of the colloidal solution.

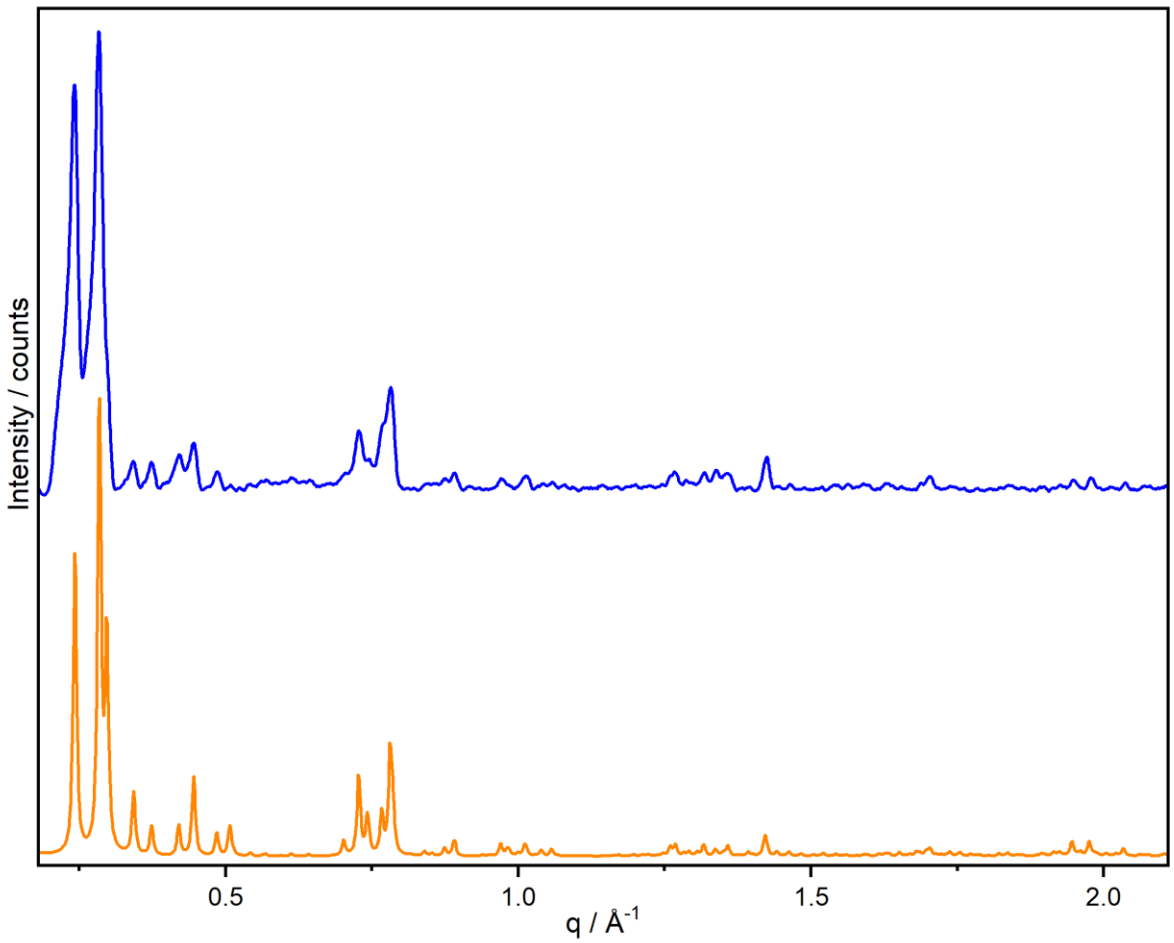

Fig. S28.

Experimental (blue) and simulated (orange) PXRD patterns of **MIL-100(Fe)** after thermal activation. Data for the calculation of the theoretical pattern were obtained from reference.[14]

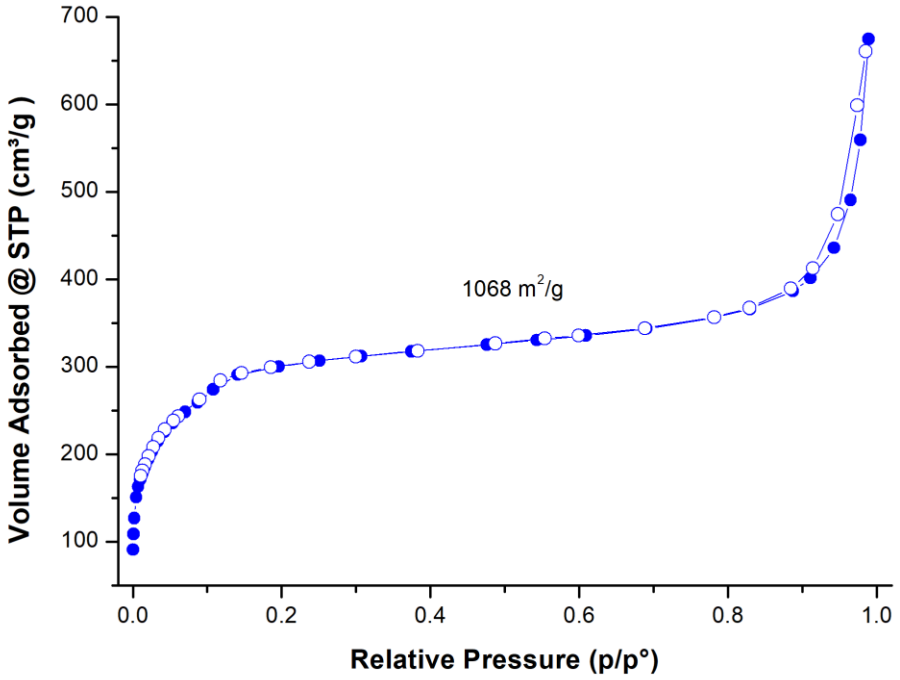

Fig. S29.

N_2 adsorption (solid dots) and desorption (open dots) isotherms of **MIL-100(Fe)** at 77K. Fits to the BET model yield a surface area of 1068 m^2/g.

Additional Characterization Data

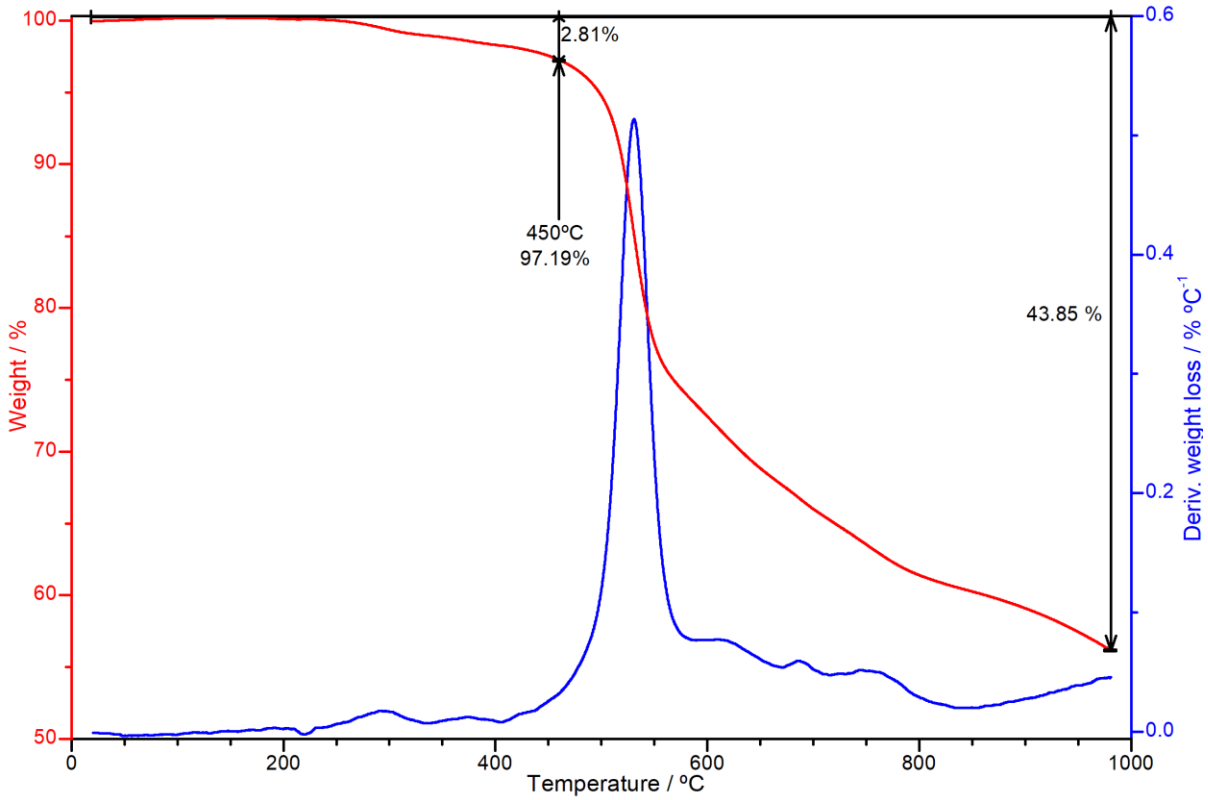

Fig. S30.
TGA trace of **TAPB-BTCA COF(s)** after critical point drying.

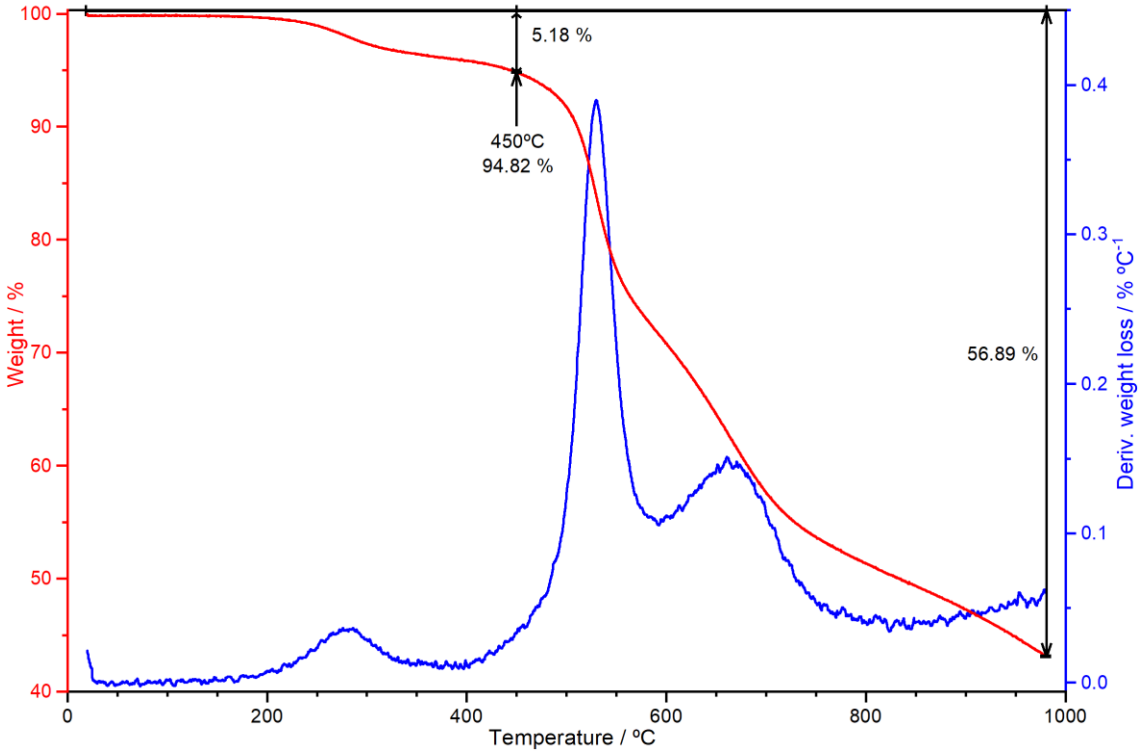

Fig. S31.
TGA trace of **Tz-COF** after critical point drying.

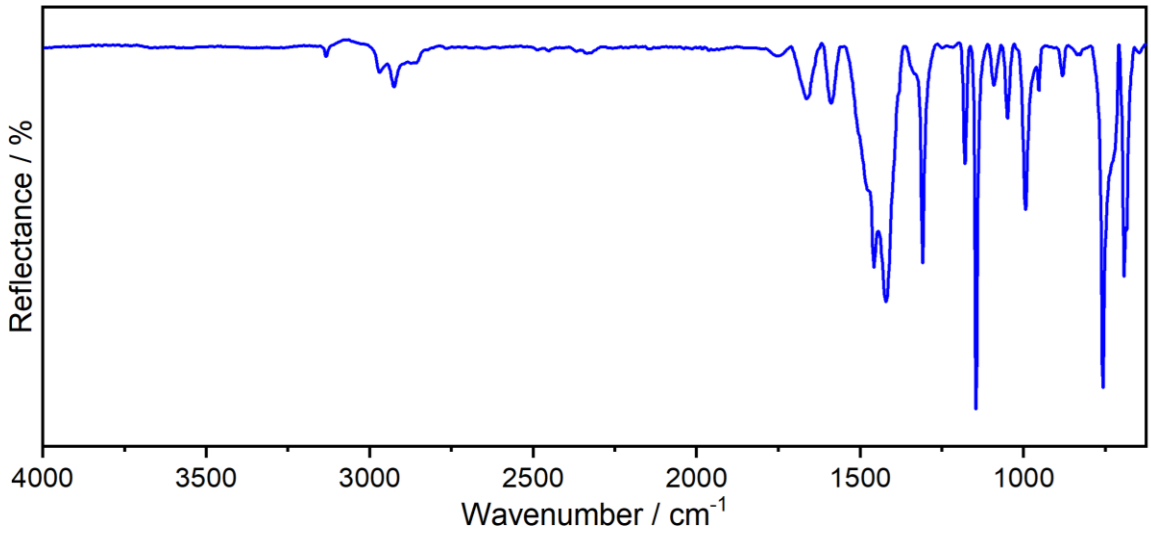

Fig. S32.

ATR-FT-IR spectrum of **MIL-100(Fe)** after thermal activation. The spectrum is highly similar to those previously reported for this MOF.[15]

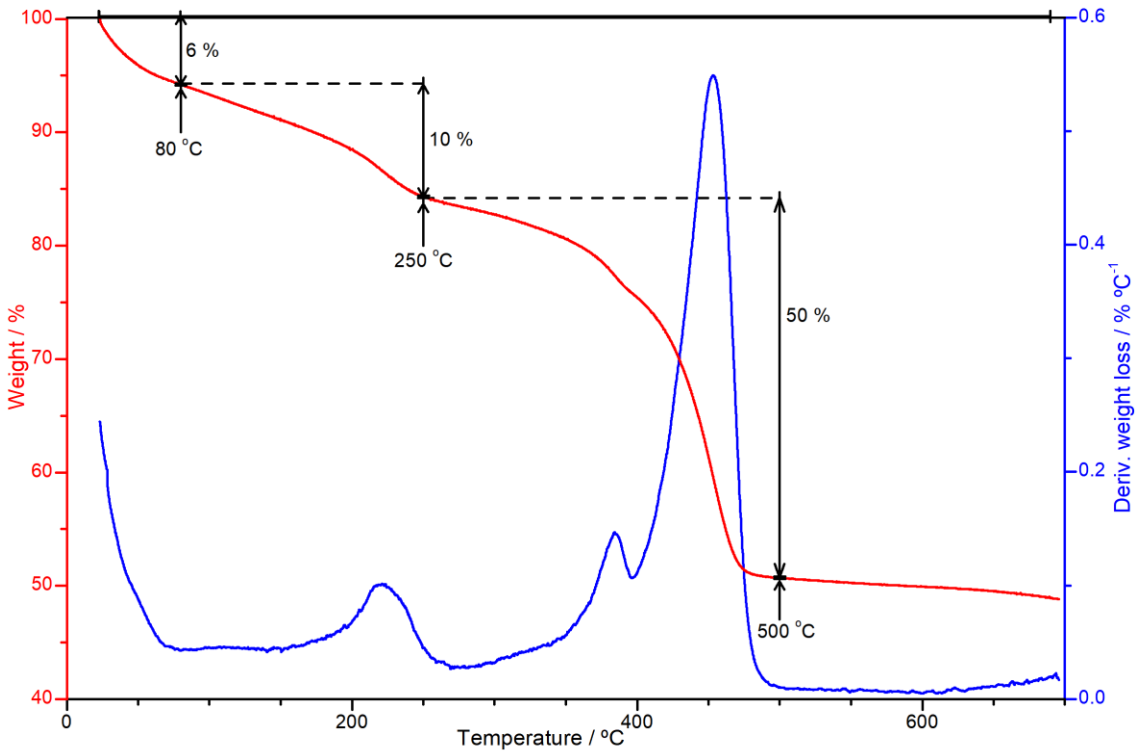

Fig. S33.

TGA trace of **MIL-100(Fe)** after thermal activation. The profile matches closely with previously reported data for this compound.[15]

Movie S1. Direct printing of TAPB-BTCA COF colloid

Movie showing the microfluidic setup employed for the printing of the **TAPB-BTCA COF** colloidal solution and the direct printing of a continuous line with **TAPB-BTCA COF** on a glass slide.

References

(1) de la Peña Ruigómez, A.; Rodríguez-San-Miguel, D.; Stylianou, K. C.; Cavallini, M.; Gentili, D.; Liscio, F.; Milita, S.; Roscioni, O. M.; Ruiz-González, M. L.; Carbonell, C.; Maspoch, D.; Mas-Ballesté, R.; Segura, J. L.; Zamora, F. Direct On-Surface Patterning of a Crystalline Laminar Covalent Organic Framework Synthesized at Room Temperature. *Chemistry – A European Journal* **2015**, *21* (30), 10666–10670. https://doi.org/10.1002/chem.201501692.

(2) Hassan, P. A.; Rana, S.; Verma, G. Making Sense of Brownian Motion: Colloid Characterization by Dynamic Light Scattering. *Langmuir* **2015**, *31* (1), 3–12. https://doi.org/10.1021/la501789z.

(3) Bail, A. L. Whole Powder Pattern Decomposition Methods and Applications: A Retrospection. *Powder Diffraction* **2005**, *20* (4), 316–326. https://doi.org/10.1154/1.2135315.

(4) Petříček, V.; Dušek, M.; Palatinus, L. Crystallographic Computing System JANA2006: General Features. *Zeitschrift für Kristallographie-Crystalline Materials* **2014**, *229* (5), 345–352.

(5) Filik, J.; Ashton, A. W.; Chang, P. C. Y.; Chater, P. A.; Day, S. J.; Drakopoulos, M.; Gerring, M. W.; Hart, M. L.; Magdysyuk, O. V.; Michalik, S.; Smith, A.; Tang, C. C.; Terrill, N. J.; Wharmby, M. T.; Wilhelm, H. Processing Two-Dimensional X-Ray Diffraction and Small-Angle Scattering Data in DAWN 2. *Journal of Applied Crystallography* **2017**, *50* (3), 959–966. https://doi.org/10.1107/S1600576717004708.

(6) Orthaber, D.; Bergmann, A.; Glatter, O. SAXS Experiments on Absolute Scale with Kratky Systems Using Water as a Secondary Standard. *Journal of Applied Crystallography* **2000**, *33*, 218–225. https://doi.org/doi:10.1107/S0021889899015216.

(7) Pedersen, J. S. Analysis of Small-Angle Scattering Data from Colloids and Polymer Solutions: Modeling and Least-Squares Fitting. *Advances in Colloid and Interface Science* **1997**, *70*, 171–210. http://dx.doi.org/10.1016/S0001-8686(97)00312-6.

(8) Marrink, S. J.; Risselada, H. J.; Yefimov, S.; Tieleman, D. P.; de Vries, A. H. The MARTINI Force Field: Coarse Grained Model for Biomolecular Simulations. *J. Phys. Chem. B* **2007**, *111* (27), 7812–7824. https://doi.org/10.1021/jp071097f.

(9) Bochicchio, D.; Kwangmettatam, S.; Kudernac, T.; Pavan, G. M. How Defects Control the Out-of-Equilibrium Dissipative Evolution of a Supramolecular Tubule. *ACS Nano* **2019**, *13* (4), 4322–4334. https://doi.org/10.1021/acsnano.8b09523.

(10) Abraham, M. J.; Murtola, T.; Schulz, R.; Páll, S.; Smith, J. C.; Hess, B.; Lindahl, E. GROMACS: High Performance Molecular Simulations through Multi-Level Parallelism from Laptops to Supercomputers. *SoftwareX* **2015**, *1–2*, 19–25. https://doi.org/10.1016/j.softx.2015.06.001.

(11) Schmitz, K. S. *Introduction to Dynamic Light Scattering by Macromolecules*; Academic Press: San Diego, 1990. https://doi.org/10.1016/C2009-0-29091-X.

(12) Bai, L.; Phua, S. Z. F.; Lim, W. Q.; Jana, A.; Luo, Z.; Tham, H. P.; Zhao, L.; Gao, Q.; Zhao, Y. Nanoscale Covalent Organic Frameworks as Smart Carriers for Drug Delivery. *Chemical Communications* **2016**, *52* (22), 4128–4131. https://doi.org/10.1039/C6CC00853D.

(13) Dong, J.; Wang, Y.; Liu, G.; Cheng, Y.; Zhao, D. Isoreticular Covalent Organic Frameworks for Hydrocarbon Uptake and Separation: The Important Role of Monomer

Planarity. *CrystEngComm* **2017**, *19* (33), 4899–4904. https://doi.org/10.1039/C7CE00344G.

(14) Horcajada, P.; Surblé, S.; Serre, C.; Hong, D.-Y.; Seo, Y.-K.; Chang, J.-S.; Grenèche, J.-M.; Margiolaki, I.; Férey, G. Synthesis and Catalytic Properties of MIL-100(Fe), an Iron(III) Carboxylate with Large Pores. *Chemical Communications* **2007**, *0* (27), 2820–2822. https://doi.org/10.1039/B704325B.

(15) Seo, Y.-K.; Yoon, J. W.; Lee, J. S.; Lee, U.-H.; Hwang, Y. K.; Jun, C.-H.; Horcajada, P.; Serre, C.; Chang, J.-S. Large Scale Fluorine-Free Synthesis of Hierarchically Porous Iron(III) Trimesate MIL-100(Fe) with a Zeolite MTN Topology. *Microporous and Mesoporous Materials* **2012**, *157*, 137–145. https://doi.org/10.1016/j.micromeso.2012.02.027.